Dalton Transactions

ROYAL SOCIETY OF CHEMISTRY

PAPER

View Article Online
View Journal | View Issue

Cite this: *Dalton Trans.*, 2026, **55**, 4269

Comparative solution study of imidazole-derived thiosemicarbazone complexes: effects of methylation and aromatic conjugation on the redox properties, anticancer, and antibacterial activity

Tatsiana V. Petrasheuskaya,[a] Márton A. Kiss,[a] Peter Rapta,[b] Csenge Fonay,[c] Nóra V. May,[c] Gabriella Spengler,[d] Éva Frank[a] and Éva A. Enyedy*[a]

A series of imidazole-based thiosemicarbazones (TSCs) was developed, and their metal complexation behavior was comprehensively investigated in solution. In addition, the structures of four ligands and four corresponding complexes were determined by single-crystal X-ray diffraction, revealing that Cu(II) and Fe(III) complexes adopt coordination through the (N,N,S) donor set. Lipophilicity, acid–base and complex formation equilibria with Cu(II), Fe(II/III), and Ni(II) were characterized using pH-potentiometry, UV-visible and electron paramagnetic resonance spectroscopy methods. Based on the solution equilibrium data, the imidazole-TSCs exist predominantly in their neutral form at physiological pH (7.4), and exhibit a stronger affinity for Cu(II) than for Fe(II), Fe(III) or Ni(II). They form mono-ligand complexes with all of these metals, and additionally tetranuclear complexes with Cu(II). The electrochemical properties of the Cu(II) complexes were characterized by cyclic voltammetry and UV-visible spectroelectrochemistry, revealing all Cu(II) complexes of imidazole-TSCs follow an electrochemical dual-pathway square scheme. The anticancer activity of imidazole-TSC derivatives was evaluated against the human cancer cell lines Colo205 and the doxorubicin-resistant Colo320. Coordination of imidazole-TSC derivatives to Cu(II) or Ni(II) markedly enhanced their anticancer activity against Colo205 and Colo320 cells. Among the compounds tested, Me_2-imidazole-TSC demonstrated the greatest potency, while the benzimidazole-TSC complex also exhibited pronounced activity. Methyl substitution and aromatic conjugation were found to substantially improve the cytotoxic effect.

Received 8th December 2025,
Accepted 17th February 2026

DOI: 10.1039/d5dt02939b

rsc.li/dalton

1 Introduction

Thiosemicarbazones (TSCs) represent a prominent class of metal-chelating agents that have been extensively investigated as potential therapeutic drugs for a wide range of human diseases, including cancer, bacterial and viral infections.[1–4] Among them, 3-aminopyridine-2-carboxaldehyde thiosemicarbazone (triapine) is the most notable example, belonging to the α-*N*-heterocyclic TSC family. It has already been evaluated in more than 35 phase I and II clinical trials for both solid and haematological malignancies.[5] Currently, a phase III clinical trial is recruiting patients to investigate the efficacy of combining triapine with cisplatin during radiotherapy.[6] Of particular note, there are two other TSCs, namely di-2-pyridylketone 4-cyclohexyl-4-methyl-3-thiosemicarbazone (DpC) and 4-(2-pyridinyl)-2-(6,7-dihydro-8(5*H*)-quinolinylidene)-hydrazide (COTI-2), which are currently undergoing phase I evaluation as anticancer agents.[7,8] The main limitation in therapeutic application of TSCs is their high toxicity, which has manifested as various side effects in clinical trials involving triapine.[9] A number of studies have demonstrated that the remarkable metal-chelating ability of TSCs often results in enhanced biological activity when coordinated to metal ions, which provides versatile pharmacological profile and multi-target properties.[10,11] The iron containing enzyme ribonucleotide reductase (RNR) is considered to be the main target of triapine and related TSCs due to their prominent iron binding ability and redox activity of the resulting metal complexes.[12] The inhibition of RNR enzymes is linked to the ability of these com-

[a]*Department of Molecular and Analytical Chemistry, University of Szeged, Dóm tér 7-8, H-6720 Szeged, Hungary. E-mail: enyedy@chem.u-szeged.hu*
[b]*Institute of Physical Chemistry and Chemical Physics, Slovak University of Technology in Bratislava, Radlinského 9, SK-81237 Bratislava, Slovakia*
[c]*Centre for Structural Sciences, HUN-REN Research Centre for Natural Sciences, Magyar tudósok körútja 2, H-1117 Budapest, Hungary*
[d]*Department of Medical Microbiology, Albert Szent-Györgyi Medical School, University of Szeged, Semmelweis utca 6, H-6725 Szeged, Hungary*

pounds to form highly stable complexes with both Fe(II) and Fe(III) ions.[13] In contrast, some other TSCs have been shown to act *via* different mechanisms, including interactions with cellular copper ions. Such interactions have been observed for certain nanomolar-active terminal *N*-disubstituted TSCs.[14,15] Moreover, Cu(II) complexes of structurally different TSCs frequently exhibit cytotoxic activity and in some cases they have been found to be more active than the free ligands, since the complexes may exert alternative modes of action. As iron, copper is also known to be redox-active under physiological conditions and can participate in redox cycling, leading to the generation of reactive oxygen species (ROS).[16] In all, the mechanism of the TSCs is associated with their ability to bind to endogenous metal ions. Moreover, it has been demonstrated that numerous synthetized Cu(II) complexes of TSCs exhibit significant *in vitro* cytotoxic activity, which can be influenced by the introduction of various substituents or ligand conjugations.[17–19] Recent studies have demonstrated that TSCs and their metal complexes can be efficiently fine-tuned through structural modifications to achieve distinct anticancer profiles. Such modifications resulted in compounds capable of mitochondria targeting, inhibition of tubulin polymerization, and circumvention of multidrug resistance, often *via* mechanisms that differ from those of conventional chemotherapeutics. These reports highlight the need of systematic investigations of structure–property–bioactivity relationships and solution behavior to enable rational design and support clinical translation.[20–24]

To explore the impact of the ligand scaffold exchange on the physico-chemical properties of TSCs, the α-*N*-pyridyl moiety can be replaced with imidazole and benzimidazole units. The imidazole moiety is a fundamental component of significant biological compounds (*e.g.*, histidine), serving as a crucial pharmacophore in numerous antiviral, antifungal, and anticancer agents. Recent studies on imidazole-derived TSCs have demonstrated their antiproliferative effects against bacteria, which are further enhanced upon coordination to copper.[20] Polypharmacological effects, including cytotoxic and antimicrobial activity, have also been reported for other TSC derivatives, and structural modifications can improve the pharmacokinetic characteristics of TSCs and optimize their solubility and bioavailability.[25] Moreover, substitution of the terminal amino group in analogous TSCs usually leads to enhanced anticancer activity and the formation of highly stable Cu(II) complexes.[26] Previously reported methylimidazole-derived TSCs exhibited anticancer activity on several cancer cell lines (A549, MDA-MB-453, LS174 and BEAS-2B). This activity was further enhanced upon coordination to Cu(II) and the presence of a dichloroacetate co-ligand.[25]

Herein, we focus on imidazole and benzimidazole-based TSCs (Chart 1), and report their complexation with various transition metal ions (Cu(II), Fe(II/III) and Ni(II)) to investigate the effect of metal binding on anticancer and antimicrobial activities. The solution phase behavior of the ligands and the complexes was investigated by means of pH-potentiometric, UV-visible (UV-vis) spectrophotometric, electron paramagnetic resonance (EPR) and ^{1}H NMR spectroscopic titrations. The isolated Cu(II) complexes were characterized by UV-vis and EPR spectroscopy, electrospray ionization mass spectrometry (ESI-MS) and single crystal X-ray diffraction (SC-XRD). As the redox behavior of the Cu(II)-TSC complexes plays a pivotal role in determining their biological activity, it was investigated by combining cyclic voltammetry (CV) and UV-vis spectroelectrochemical studies. Finally, the anticancer and antimicrobial activities of the imidazole-TSC derivatives and their Cu(II) and Ni(II) complexes were tested against two human cancer cell lines *via* cytotoxicity assays and against various Gram-positive and Gram-negative bacterial strains, respectively.

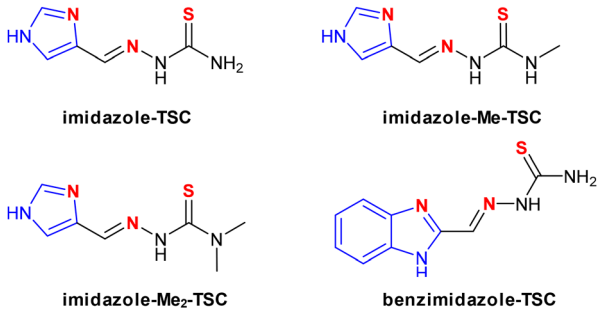

Chart 1 Chemical structures of imidazole- and benzimidazole-TSCs in neutral (HL) form.

2 Results and discussion

2.1 Synthesis of ligands imidazole-TSC, imidazole-Me-TSC, imidazole-Me$_2$-TSC and benzimidazole-TSC

Tridentate thiosemicarbazone ligands (imidazole-TSC, imidazole-Me-TSC and imidazole-Me$_2$-TSC) were synthesized from commercially available 1*H*-imidazole-4-carbaldehyde (**1**) with thiosemicarbazide, 4-methyl-thiosemicarbazide and 4,4-dimethyl-thiosemicarbazide, respectively (Scheme 1). 1*H*-Benzimidazole-2-carbaldehyde (**2**) was prepared as previously

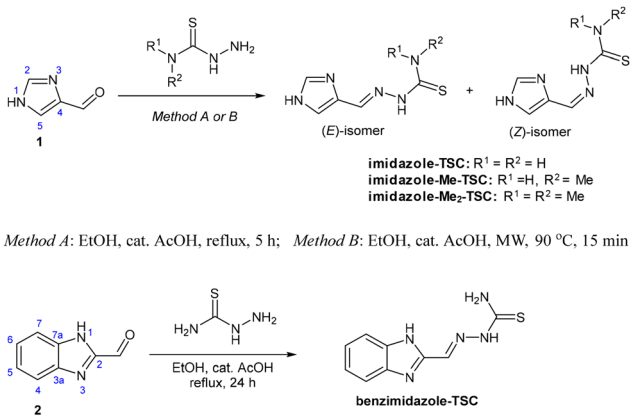

Scheme 1 Synthesis of imidazole-TSC, imidazole-Me-TSC, imidazole-Me$_2$-TSC and benzimidazole-TSC (abbreviations: EtOH: ethanol, AcOH: acetic acid, MW: microwave).

described[27,28] and converted to its corresponding TSC derivative using thiosemicarbazide. For the imidazole-TSCs, the condensation reactions were performed in the presence of a catalytic amount of glacial acetic acid (AcOH), either by heating the reactants under reflux in absolute ethanol (EtOH) (Method A)[29] or by microwave (MW) irradiation (Method B). The MW-assisted transformations carried out in a closed vessel in a manner similar to the conventional method but at a slightly higher temperature (90°C) than the boiling point of EtOH (78 °C), markedly reduced the reaction time (15 min). For benzimidazole-TSC, only conventional heating was employed; the reaction proceeded much more slowly and required 24 h of reflux to achieve sufficient conversion. After purification by column chromatography, the TSCs (imidazole-TSC, imidazole-Me-TSC, imidazole-Me_2-TSC and benzimidazole-TSC) were obtained in a crystalline form in moderate to high yields. The ^{1}H NMR spectra recorded in DMSO-d_6, revealed that (*E*/*Z*) isomerization, commonly observed for substituted hydrazones and thiosemicarbazones,[30,31] occurred in solution for the monocyclic products. The spectrum of imidazole-Me_2-TSC, recorded immediately after dissolution, showed the almost exclusive presence of the (*E*)-isomer, however, over time, the (*Z*)-isomer began to predominate. At equilibrium, the isomeric ratio was approximately 30 : 70 in favor of the (*Z*)-form (for all imidazole derivatives). To determine the configuration of the products resulting from the condensations, the chemical shifts of the CH=N proton signals of the related isomers were compared. According to the Karabatsos rule, the proton attached to the imine carbon in aldehyde hydrazones is more deshielded when it is *cis* to the residual NH moiety than when it is *trans*.[31] Similar (*E*/*Z*)-isomerization was not detected in the case of benzimidazole-TSC.

The structures of the thiosemicarbazones were confirmed by ^{1}H and ^{13}C NMR as well as 2D NMR (HSQC, HMBC) measurements (see spectra in Fig. S1–S13 in SI), in addition to electrospray ionization mass spectrometry (ESI-MS) (Fig. S14–S17). The protonated molecular ions $[M + H]^+$ were occasionally observed in the MS spectra, while compounds with primary amine moiety showed additional $[M + H - NH_3]^+$ fragments. However, the spectra were often dominated by mono- and bis-ligand iron complex ions ($[M + Fe - H]^+$ and $[2M + Fe - 2H]^+$), which are attributed to in-source complex formation during the ESI process. Among the synthesized compounds, imidazole-TSC[30] and benzimidazole-TSC,[32] the latter lacking experimental details, have been reported previously, while imidazole-Me-TSC and imidazole-Me_2-TSC are described here for the first time.

2.2 *In vitro* cytotoxicity and antibacterial activity of the TSCs and the impact of the complexation with Cu(II) and Ni(II)

Methylimidazole-derived TSCs showed anticancer effects against various cancer cell lines (A549, MDA-MB-453, LS174 and BEAS-2B) in previous studies, and these effects were further enhanced upon the coordination to Cu(II) and the presence of dichloroacetate as a co-ligand.[25] Based on this finding, anticancer activity of the title compounds was investigated using the colorimetric MTT assay on a chemosensitive (Colo205) and doxorubicin resistant (Colo320) colon adenocarcinoma cells with a 72 h exposure time. As metal chelation may enhance the anticancer activity of TSCs, these studies were also performed with equimolar amounts of $CuCl_2$ and $NiCl_2$, and the obtained IC_{50} values are shown in Table 1. The results demonstrated that the ligands alone were non-cytotoxic or only weakly cytotoxic toward the cancer cells tested, with the exception of Me_2-imidazole-TSC, which exhibited a notable level of activity on both Colo205 and Colo320 cells. It is noteworthy that the reference compound triapine, bearing 3-aminopyridine moiety, exhibited significantly stronger cytotoxicity toward the same cell lines under identical experimental conditions (IC_{50} = 3.28 and 2.17 μM on Colo205 and Colo320, respectively).[33]

In the presence of Cu(II) and Ni(II), the activity of the benzimidazole-TSC was significantly increased, and the obtained IC_{50} values were much lower than those of the corresponding metal salts. For imidazole-TSC and imidazole-Me-TSC, the addition of the metal salts also induced higher anticancer activity; however, in some of these cases the IC_{50} values were comparable to those observed with the metal salts alone. As imidazole-Me_2-TSC exhibited the strongest cytotoxicity among the tested ligands against these cancer cell lines, this compound and its complexes were further evaluated in the non-cancerous MRC-5 fibroblast cell line to assess their selectivity (Table 1). Imidazole-Me_2-TSC showed considerable selectivity toward cancer cells, with *ca.* a three-fold increase in IC_{50} values observed in fibroblasts. Whereas the corresponding metal complexes were more cytotoxic toward the non-cancerous cells.

In addition, antibacterial activity was also tested on the Gram-positive *Staphylococcus aureus* and the Gram-negative *Escherichia coli* and *Klebsiella quasipneumoniae* strains.

Table 1 *In vitro* cytotoxic effect (IC_{50} values in μM) of imidazole-TSC, imidazole-Me-TSC, imidazole-Me_2-TSC and benzimidazole-TSC, evaluated both in the absence and presence of one equivalent of Cu(II) and Ni(II), as well as for the controls (metal salt, doxorubicin) in Colo205 and Colo320 cancer cell lines and in MRC-5 non-cancerous cells. (n.d. = not determined). {72 h exposure}

	Colo205 IC_{50} (μM)	Colo320	MRC-5
Imidazole-TSC	84.4 ± 9.3	90.3 ± 6.0	n.d.
Imidazole-Me-TSC	98.5 ± 7.7	88.5 ± 3.9	n.d.
Imidazole-Me_2-TSC	9.98 ± 0.37	8.97 ± 0.33	29.0 ± 1.5
Benzimidazole-TSC	>100	>100	n.d.
Imidazole-TSC + Cu(II)	28.8 ± 1.9	58.6 ± 4.2	n.d.
Imidazole-Me-TSC + Cu(II)	38.75 ± 0.84	56.3 ± 2.4	n.d.
Imidazole-Me_2-TSC + Cu(II)	14.5 ± 1.7	28.2 ± 1.3	10.8 ± 1.5
Benzimidazole-TSC + Cu(II)	25.61 ± 0.74	15.70 ± 0.71	n.d.
Imidazole-TSC + Ni(II)	32.75 ± 0.68	51.7 ± 1.6	n.d.
Imidazole-Me-TSC + Ni(II)	19.96 ± 0.15	30.7 ± 1.2	n.d.
Imidazole-Me_2-TSC + Ni(II)	40.2 ± 2.3	32.7 ± 4.0	15.5 ± 1.4
Benzimidazole-TSC + Ni(II)	10.6 ± 1.4	9.8 ± 1.2	n.d.
$CuCl_2$	42.0 ± 2.6	58.0 ± 7.2	43.5 ± 2.0
$NiCl_2$	30.4 ± 3.8	50.2 ± 1.1	18.9 ± 1.6
Doxorubicin	0.17 ± 0.02	0.55 ± 0.04	0.17 ± 0.02

The results (Table S1) demonstrated that only moderate activity on *S. aureus* was observed for imidazole-Me$_2$-TSC and the complexes of imidazole-Me$_2$-TSC and benzimidazole-TSC, while the minimal inhibitory concentration (MIC) was >100 μM for all other compounds.

In order to gain a deeper understanding of the differences between the biological activities of the ligands and the influence of the complexation on their behavior, a detailed solution equilibrium study was conducted.

2.3 Proton dissociation processes, lipophilicity and solubility of the studied thiosemicarbazones

The physico-chemical properties of biologically active compounds, including aqueous solubility, lipophilicity, actual protonation state and charge, significantly influence their bioavailability and pharmacokinetic behavior. As a preliminary step, the lipophilicity and solubility of the ligands were characterized at pH 7.4. The aqueous solubility (S) values and logarithmic distribution coefficients ($\log D_{7.40}$) were determined, presented in Table 2. The following trend in the solubility was found: imidazole-TSC > imidazole-Me-TSC > imidazole-Me$_2$-TSC > benzimidazole-TSC. The obtained distribution coefficients indicate that methyl group introduction and benzene ring annulation increase the lipophilic character, as expected. (Notably, for benzimidazole-TSC only a threshold limit could be estimated due to its high value.) Imidazole-TSC and its mono- and dimethylated derivatives are less, whereas benzimidazole-TSC is much more lipophilic than 2-formylpyridine thiosemicarbazone (FTSC),[34] the α-*N*-pyridyl TSC analogue of imidazole-TSC, at pH 7.4.

In order to gain insight into the proton dissociation processes of the ligands, pH-potentiometric titrations were conducted in 30% (v/v) DMSO/H$_2$O at 1–2 mM concentrations. (At this concentration, not all compounds were soluble in water without DMSO.) Although, the protonated ligands have three dissociable protons, namely two on the imidazolium- and one on the hydrazonic nitrogens, only two pK_a values (pK_{a1} and pK_{a2}, Table 2) could be determined. pK_{a1} is attributed to the deprotonation process of one of the imidazolium nitrogens (N3), which is involved in the coordination to Cu(II) (Chart 1), while pK_{a2} belongs to the hydrazonic nitrogen.

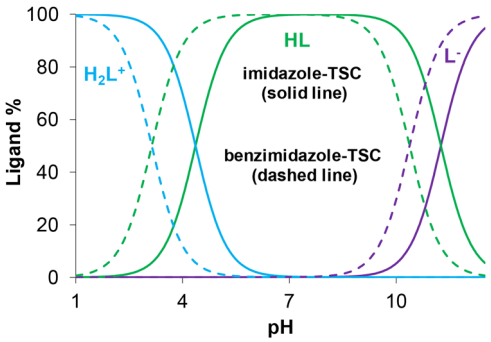

Fig. 1 Concentration distribution curves at various pH values for imidazole-TSC (solid lines) and benzimidazole-TSC (dashed line). {c_L = 1 mM; 30% (v/v) DMSO/H$_2$O; I = 0.10 M (KCl); T = 25.0 °C}.

The benzimidazole derivative possesses lower pK_a values than the imidazole derivatives (also represented by the concentration distribution curves, Fig. 1), which can be explained by the electron-withdrawing effect of the fused benzene ring, while the N-terminal monomethylation has only a minor effect on the proton dissociation constants.

In contrast, dimethylation results in lower pK_{a2} value associated with the hydrazonic nitrogen, consistent with observations reported for analogous TSCs such as derivatives of triapine, FTSC, and sterane-based-TSC hybrids.[35–37] This effect is most probably due to the reduced stabilization of the neutral thione tautomeric form of the ligand, as the dimethylation eliminates the potential intra- and intermolecular hydrogen bonding.[35–37] It should be noted that imidazole-TSC has somewhat higher pK_a values in comparison with FTSC, the simplest α-*N*-pyridyl TSC (Table 2). In all cases, the neutral HL form of these compounds predominates at pH 7.4.

The ligand imidazole-TSC possessing the best aqueous solubility was selected for ^{1}H NMR spectroscopic titrations as a representative member of the ligand series (Fig. 2) to reveal its deprotonation processes and identification of isomers in 30% (v/v) DMSO-d_6/H$_2$O solvent mixture.

The presence of both (E) and (Z) isomers arising from the C=N double bond was clearly observed in this medium, similarly to what was seen as in pure DMSO-d_6 (Fig. S1–S4). The CH2 and CH5 proton resonances (■ and * in Fig. 2, respectively) were found to be highly sensitive to the presence of the isomers and their proton dissociation processes. Only one type of isomer (identified as the major (Z) isomeric form) was observed at pH 1.31. This isomer remained predominant across the entire pH range studied; however, the minor isomer (E) appeared at pH > 3.2, as the first deprotonation began, and its fraction gradually increased to ~20% at 8.5, after which it remained practically constant. The molar fraction of this minor isomer was higher (~30%) in DMSO-d_6. The identification of the isomers was based on their characteristic resonances and their pK_a values. For the first deprotonation step, the proton dissociation constant could be determined only for

Table 2 Protonation ($\log \beta$ HL) and proton dissociation constants (pK_a)[a] of the studied ligands determined by pH-potentiometric titrations in 30% (v/v) DMSO/H$_2$O {I = 0.1 M (KCl), solubility ($S_{7.4}$) in H$_2$O and their n-octanol/water distribution coefficients ($\log D_{7.4}$ values) at T = 25 °C}[a]

	Imidazole-TSC	Imidazole-Me-TSC	Imidazole-Me$_2$-TSC	Benzimidazole-TSC
$\log \beta$ HL	11.26 ± 0.02	11.48 ± 0.04	10.85 ± 0.01	10.38 ± 0.02
$\log \beta$ H$_2$L$^+$	15.62 ± 0.02	15.97 ± 0.05	15.30 ± 0.01	13.51 ± 0.05
pK_{a1}	4.36	4.49	4.45	3.13
pK_{a2}	11.26	11.48	10.85	10.38
$\log D_{7.4}$	+0.03 ± 0.03	+0.64 ± 0.02	+0.25 ± 0.02	> +2
$S_{7.4}$	4.1 mM	2.1 mM	0.94 mM	0.12 mM

[a] Data of FTSC (for comparison): pK_{a1}(pyridinium-NH$^+$) = 3.10; pK_{a2}(hydrazonic-NH) = 11.22 in 30% (v/v) DMSO/H$_2$O; $\log D_{7.4}$ = +0.73.[34]

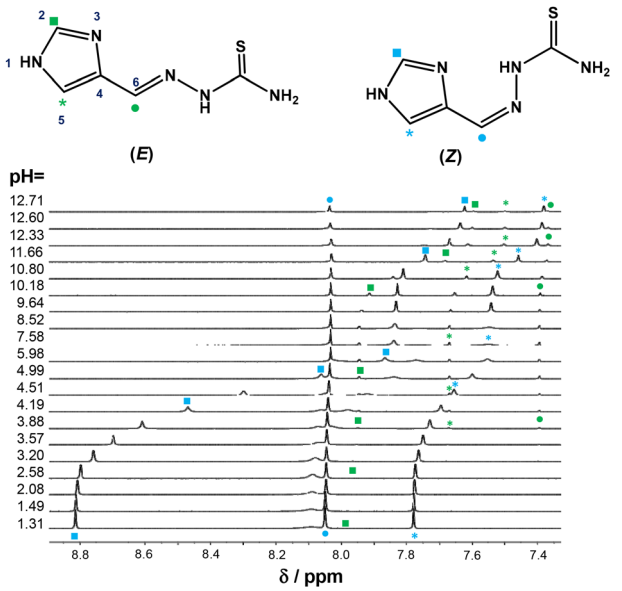

Fig. 2 ^{1}H NMR spectra of imidazole-TSC at various pH values with symbols used for proton resonances assignment in case of the major *Z* isomer (blue symbols) and minor *E* isomer (green symbols), where ligand is shown in its HL form. {c_L = 3 mM; *I* = 0.1 M (KCl); *T* = 25 °C; 30% (v/v) DMSO-d_6/H_2O}.

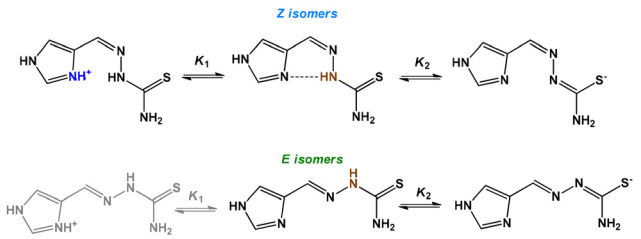

Scheme 2 (a) Electrochemical dual-pathway square scheme, where L indicates the tested ligands, reported in our former work,[37] and (b) a more complex scheme suggested for the Cu(II)–imidazole-Me_2-TSC system.

the major (*Z*) isomer (pK_{a1} = 4.47 ± 0.03), since the fraction of the minor isomer was low in this pH range, and resonances of its H_2L^+ form could not be assigned. Whereas for the second deprotonation step (at pH > 10), pK_{a2} values of 11.18 ± 0.03 and >11.5 were obtained for the minor and major isomers, respectively. The higher pK_a value of the isomer (*Z*) is likely due to intramolecular hydrogen bonding between the imidazole (N3) nitrogen and the protonated hydrazone nitrogen atoms in its HL form (Scheme 2), thus hindering the deprotonation.

2.4 Complex formation of imidazole-TSC derivatives with Cu(II), Ni(II) and Fe(II/III) metal ions

The complex formation processes of imidazole- and benzimidazole-TSC derivatives with Cu(II) ions were investigated by pH-potentiometry, and complemented by UV-vis and EPR spectroscopic measurements (for Cu(II)), in order to confirm the speciation models and to obtain information on the coordination modes in 30% (v/v) DMSO/H_2O. The overall stability constants (log β) and pK_a values of the studied Cu(II) complexes are collected in Table 3. Data obtained from pH-potentiometric titrations of the Cu(II)–imidazole-TSC system revealed that the complex formation is essentially complete even at the starting pH value of the measurements (pH = 2).

Table 3 Overall stability constants (log β), pK_a of the Cu(II) complexes of TSCs determined by UV-vis titrations in 30% (v/v) DMSO/H_2O and calculated pCu values at pH 5.0 using c_{Cu} = 20 μM and c_L = 20 μM together with FTSC for comparison;[a] (n.d. = not determined). {*T* = 25 °C; *I* = 0.1 M (KCl)}

	Imidazole-TSC	Imidazole-Me-TSC	Imidazole-Me_2-TSC	Benzimidazole-TSC
Log β $[CuLH]^{2+}$	19.87 ± 0.01	19.48 ± 0.02	19.47 ± 0.05	n.d.
Log β $[CuL]^+$	17.25 ± 0.02	16.82 ± 0.02	16.68 ± 0.05	14.04 ± 0.01
Log β $[Cu_4L_4H_{-4}]$	56.89 ± 0.07	56.78 ± 0.08	n.d.	41.28 ± 0.04
Log β $[CuLH_{-2}]^-$	2.29 ± 0.04	n.d.	n.d.	−2.91 ± 0.02
pK_a $[CuLH]^{2+}$	2.62	2.66	2.79	n.d.
$pCu_{5.0}$	7.9	7.5	7.8	6.8

[a] The UV-vis titrations were performed with imidazole-TSC at ~110 μM, while with the other derivatives at ~20 μM concentrations. FTSC: $pCu_{5.0}$ = 6.6 under the same conditions.[34]

Therefore, UV-vis spectra were also recorded in the pH range 1–2 for all compounds studied. (To maintain constant ionic strength, samples were prepared by gradually exchange KCl to HCl, and the actual pH was calculated based on the concentration of the strong acid.) The spectrum recorded at pH 1.59 represents significant complex formation, as it is completely different from the spectrum of the free ligand (Fig. 3a). At this pH, $[CuLH]^{2+}$ is formed and its formation is completed to pH ~ 2.7. Increasing the pH, the subsequent process starts, which corresponds to the formation of $[CuL]^+$ species (Fig. 3a).

Remarkable spectral changes were observed in the pH range of 5–7 in the equimolar solution, which is attributed to metal-induced deprotonation process of the non-coordinated imidazole nitrogen (NH^1), typically considered non-dissociable within this pH range, and to the formation of a tetrameric species, $[Cu_4L_4H_{-4}]$ (as shown in Fig. 3b).

The formation of this species is supported by literature data, in which similar tetranuclear structures have been reported for Cu(II) complexes with imidazole derivatives in solution.[38–40] Moreover, ESI-MS analysis revealed the presence of a dimeric species for all isolated Cu(II) complexes (*vide infra*), which most likely formed due to the dissociation of the tetramer under the conditions of the ESI-MS experiment (Fig. S18–S21). It is noteworthy that the formation of the trinuclear $[Cu_3L_2]^{2+}$ species was reported for triapine and related ligands; however, such complexes are formed only under the condition of ligand excess.[41] In contrast, equimolar solutions of tridentate α-*N*-pyridyl or salicylaldehyde TSCs yield only monomeric mono-ligand Cu(II) complexes.[42] An additional

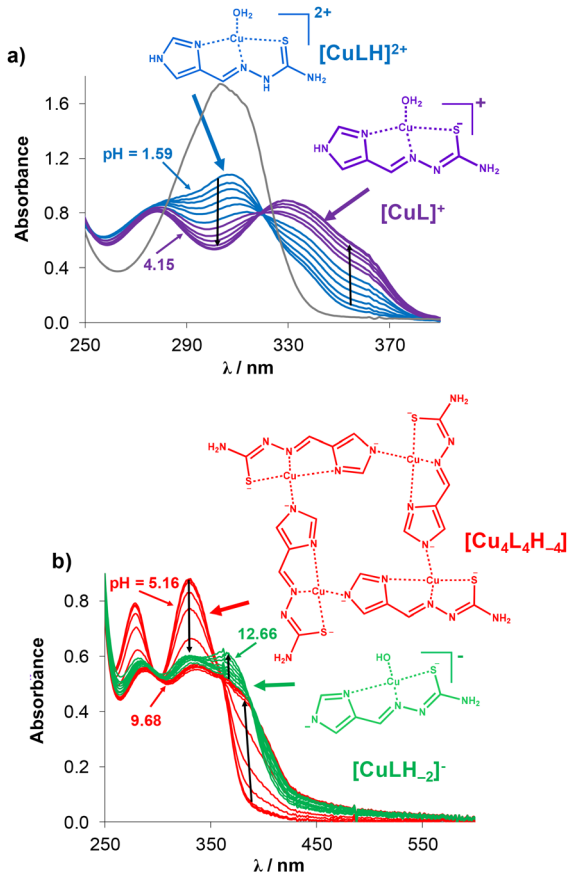

Fig. 3 UV-vis absorption spectra recorded for the Cu(II)–imidazole-TSC (1 : 1) system in the pH range (a) 1.59–4.15 together with the spectrum of the ligand at pH 1.79 (grey line), and (b) between pH 5.16 and 12.66 in 30% (v/v) DMSO/H_2O together with the suggested structures of species formed. {c_L = 117 μM; c_{Cu} = 114 μM; I = 0.1 M (KCl); T = 25.0 °C; ℓ = 0.5 cm}.

process was observed at pH > 9, which most probably corresponds to the formation of a mixed hydroxido complex $[CuLH_{-2}]^-$. In this species, the tridentate TSC ligand binds *via* its (N,N,S$^-$) donor set, while an OH^- ligand is coordinated at the fourth equatorial position, as depicted in Fig. 3b.

Concentration distribution curves were computed for the Cu(II)–imidazole-TSC (1 : 1) system using the obtained formation constants (Fig. 4), and it can be seen that $[CuLH]^{2+}$ and $[CuL]^+$ are the predominant species in the acidic pH range. $[Cu_4L_4H_{-4}]$ species was found predominant in the pH range 5–9 (also including the physiological pH), while $[CuLH_{-2}]^-$ species was the most abundant at pH > 10. $[CuLH]^{2+}$ contains the protonated HL ligand, where the proton is present on the non-coordinating hydrazonic nitrogen. In the $[CuL]^+$ complex the deprotonated ligand coordinates most probably *via* the ($N_{imidazole}$,N,S$^-$) tridentate donor set. Moreover, these suggested coordination modes in species $[CuLH]^{2+}$ and $[CuL]^+$ were confirmed by SC-XRD (Section 2.6). It is worth mentioning that only $[CuLH]^{2+}$ and $[CuL]^+$ species could be detected for imidazole-Me_2-TSC as precipitation occurred at pH > 6.0, which hindered further data evaluation.

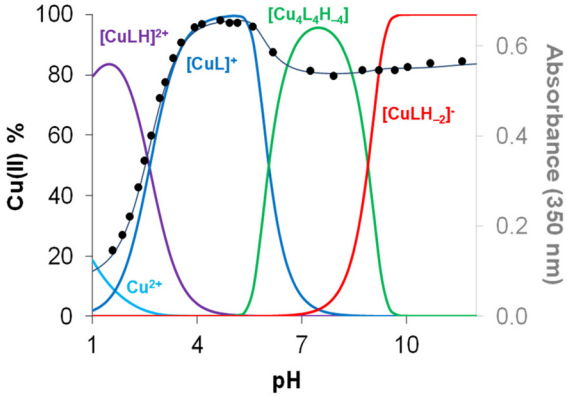

Fig. 4 Concentration distribution curves for the Cu(II)–imidazole-TSC (1 : 1) system plotted together with the absorbance changes at 350 nm (●) with the fitted curve (dotted line) {c_{ligand} = 117 μM; $c_{Cu(II)}$ = 114 μM; 30% (v/v) DMSO/H_2O; T = 25.0 °C; I = 0.1 M (KCl); ℓ = 0.5 cm}.

To better understand and confirm the proposed coordination modes of the Cu(II) – complexes, the Cu(II)–imidazole-TSC system was studied by EPR spectroscopy. Spectra were recorded at 1 : 1 and 1 : 2 metal-to-ligand ratios at different pH values in 30% (v/v) DMSO/H_2O both at room temperature and 77 K. A series of frozen solution EPR spectra were recorded and evaluated between pH 1–7, while at pH > 7 the EPR signal intensity decreased significantly. This is most likely due to signal broadening effect caused by coupling between closely located Cu(II) centers arising from tetramer formation and subsequent precipitation at elevated pH.

The measured and simulated spectra are shown together in Fig. 5a and b. The EPR parameters of the obtained components are summarized in Table 4 and their calculated spectra are shown in Fig. 5c.

The EPR spectra indicate that complexation begins at very low pH; the fraction of free copper ($[Cu(H_2O)_6]^{2+}$) was less than 20% even at pH ~ 1.2. The $[CuLH]^{2+}$ complex already shows high ligand field around Cu(II), and the observed nitrogen splitting further supports coordination of two nitrogen atoms, suggesting that the ligand binds in a tridentate ($N_{imidazole}$,N,S) coordination mode. Deprotonation of the hydrazine-NH caused only a slight effect in the EPR spectrum, however, based on the decrease in g_z and the increase in A_z, $[CuL]^+$ could be distinguished from $[CuLH]^{2+}$.

At ligand excess, a new species appeared under acidic conditions, most likely corresponding to the $[CuL_2H_2]^{2+}$ complex. The well-resolved nitrogen splitting could be fitted by assuming that two nitrogen atoms coordinate from the '*x*' direction of the *g*-tensor. This suggests that, in this bis-ligand complex, the S and hydrazine-NH groups of both ligands can bind to the Cu(II) center in *trans* position. At pH ≳ 4, deprotonation of the coordinated ligands leads to the formation of $[CuL_2]$, with the accompanying spectral changes indicating a rearrangement of the coordination sphere. These observations imply that one of the ligand probably coordinates in a tridentate manner, while the second ligand adopts an equatorial–axial binding mode to

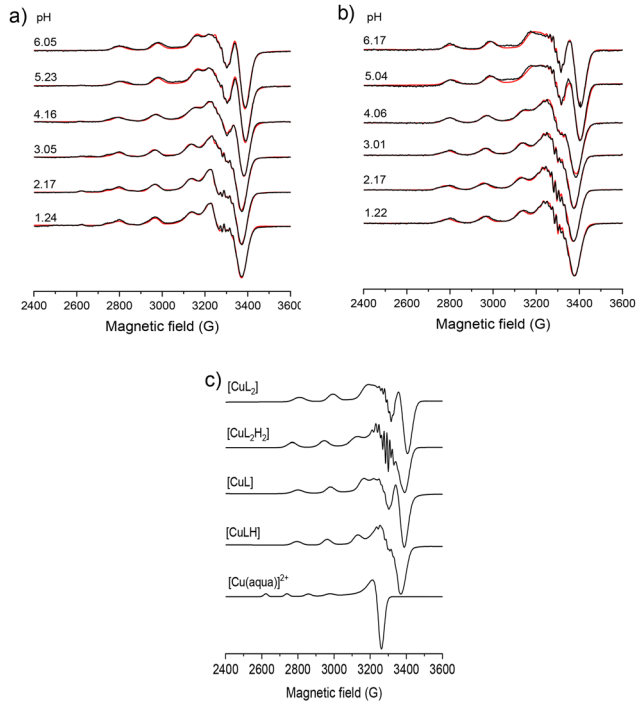

Fig. 5 Experimental (black) and simulated (red) anisotropic frozen solution EPR spectra obtained in 30% (v/v) DMSO/H_2O for the Cu(II)–imidazole-TSC system at (a) equimolar ratio and (b) metal-to-ligand ratio of 1 : 2 (two-fold ligand excess). (c) Component anisotropic EPR spectra obtained for the same system.

Table 4 Anisotropic EPR parameters of the copper(II) complexes of imidazole-TSC. Coupling values are shown in 10^{-4} cm^{-1} units[a]

Component	$[CuLH]^{2+}$	$[CuL]^{+}$	$[CuL_2H_2]^{2+}$	$[CuL_2]$	$[Cu(aqua)]^{2+}$
g_x	2.035	2.034	2.028	2.029	2.081
g_y	2.051	2.058	2.061	2.051	2.081
g_z	2.213	2.196	2.223	2.185	2.408
A_x	27	27	32	24	9
A_y	15	24	20	26	9
A_z	169	181	180	184	128
a_x^{N1}	15	13	18	11	—
a_y^{N1}	15	14	14	17	—
a_z^{N1}	15	11	9	16	—
n(N1)	1	1	1	1	—
a_x^{N2}	13	15	18	14	—
a_y^{N2}	19	10	14	10	—
a_z^{N2}	9	11	9	14	—
n(N2)	1	1	1	2	—
$g_{0,calc.}$[b]	2.1	2.096	2.104	2.088	2.19

[a] The experimental error were ±0.002 for g_x and g_y and ±0.001 for g_z, ±2 × 10^{-4} cm^{-1} for A_x and A_y and ±1 × 10^{-4} cm^{-1} for A_z. [b] Calculated by the equation $g_{0,calc} = (g_x + g_y + g_z)/3$.

the Cu(II) ion. The nitrogen lines in the spectra were best fitted by assuming the coordination of three nitrogen donor atoms in the equatorial plane. The ratios of the components at different pH values, as obtained by the simulation of frozen solution EPR spectra are shown in Fig. S22.

In order to compare the intrinsic Cu(I)-binding ability of the investigated ligands in solution, pCu values were calculated at pH 5.0, where no precipitation occurred in any of the systems (Table 3). pM is the negative decadic logarithm of the equilibrium concentration of the free (unbound) metal ion (M). Thus, higher values indicate higher stability of the complexes in solution under the given conditions. The results indicate that only minor differences exist between the calculated pCu values for the studied imidazole-TSCs ($pCu_{5.0}$ = 7.5–7.9), and that N-terminal substitution does not significantly affect complex stability. However, a lower value was obtained for benzimidazole-TSC ($pCu_{5.0}$ = 6.8). In contrast, FTSC and triapine exhibits lower pCu values ($pCu_{5.0}$ = 6.6 and 6.4, respectively[34,41]), indicating that substitution of the pyridine ring with an imidazole moiety significantly increases the Cu(II)-binding affinity at pH 5.0.

In order to gain a deeper understanding of the differences in anticancer activity among the ligands, and to assess the influence of complexation with Ni(II) ions on their behavior, a solution equilibrium study was also conducted with this metal ion. Furthermore, complexation with Fe(II/III) ions was also investigated, as α-N-heterocyclic TSCs are known to form stable, redox active complexes with both iron ions. These complexes are capable of activating molecular oxygen, resulting in the generation of reactive oxygen species that can induce cellular damage. For this reason, pH-potentiometric titrations were conducted in 30% (v/v) DMSO/H_2O and at different metal-to-ligand ratios (1 : 1, 1 : 1.5, 1 : 2 and 1 : 3).

Imidazole-TSC was selected as the ligand for comparison due to its highest solubility, with the aim of evaluating the stability of the complexes in solution. The overall stability constants of the complexes, providing the best fits to the experimental data are presented in Table 5. To determine the stoichiometry and formation constants of the Ni(II) complexes with imidazole-TSC, pH-potentiometric titrations were carried out in the pH range 2–9, since hydrolysis at alkaline pH values suppressed complex formation and led to precipitation. Analysis of the titration data revealed that only monoligand species, $[NiLH]^{2+}$ and $[NiL]^{+}$, are formed. Taking into account the concentration distribution curves computed (Fig. 6), the complex formation of $[NiLH]^{2+}$ begins at pH 2, while $[NiL]^{+}$ appears at pH > 4. This indicates that the ligand has a significantly weaker affinity for Ni(II) compared to Cu(II).

For the Fe(II) and Fe(III) complexes, pH-potentiometric titrations were performed over the same pH range, due to hydrolysis, similarly to the pH-potentiometric titrations conducted for the Ni(II) containing samples. The studied imidazole-TSC formed both mono- and bis-ligand complexes with both Fe(II) and Fe(III), similarly to other related tridentate α-*N*-pyridyl-TSCs, such as triapine and its derivatives.[43] Namely, $[Fe(II)LH]^{2+}$, $[Fe(II)L]^{+}$ and $[Fe(II)L_2]$ species were found for Fe(II) and $[Fe(III)L]^{2+}$, $[Fe(III)L_2]^{+}$ and $[Fe(III)L_2H_{-1}]$ were identified with Fe(III).

In these complexes, the coordination of the ligand *via* the (N,N,S^{-}) donor set was suggested which was confirmed by X-ray crystallography for the Fe(III)–imidazole-Me_2-TSC complex (see Section 2.6).

Table 5 Overall stability constants (log β) of the Fe(II), Fe(III) and Ni(II) complexes of imidazole-TSC determined by pH-potentiometric titrations in 30% (v/v) DMSO/H_2O{T = 25 °C; I = 0.1 M (KCl)}

Log β of Fe(II) complexes		Log β of Fe(III) complexes		Log β of Ni(II) complexes	
$[Fe(II)LH]^{2+}$	14.78 ± 0.05	$[Fe(III)L]^{2+}$	13.52 ± 0.02	$[Ni(II)LH]^{2+}$	14.59 ± 0.09
$[Fe(II)L]^{+}$	7.90 ± 0.09	$[Fe(III)L_2]^{+}$	25.58 ± 0.04	$[Ni(II)L]^{+}$	8.84 ± 0.07
$[Fe(II)L_2]$	15.06 ± 0.07	$[Fe(III)L_2H_{-1}]$	17.60 ± 0.09		

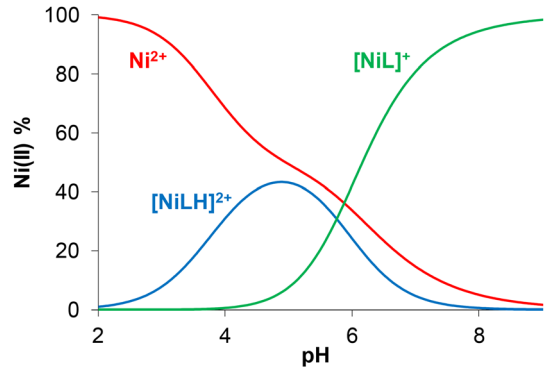

Fig. 6 Concentration distribution curves for the Ni(II)–imidazole-TSC (1 : 1) system {c_{ligand} = 1 mM; $c_{Ni(II)}$ = 1 mM; 30% (v/v) DMSO/H_2O; T = 25.0 °C; I = 0.1 M (KCl)}.

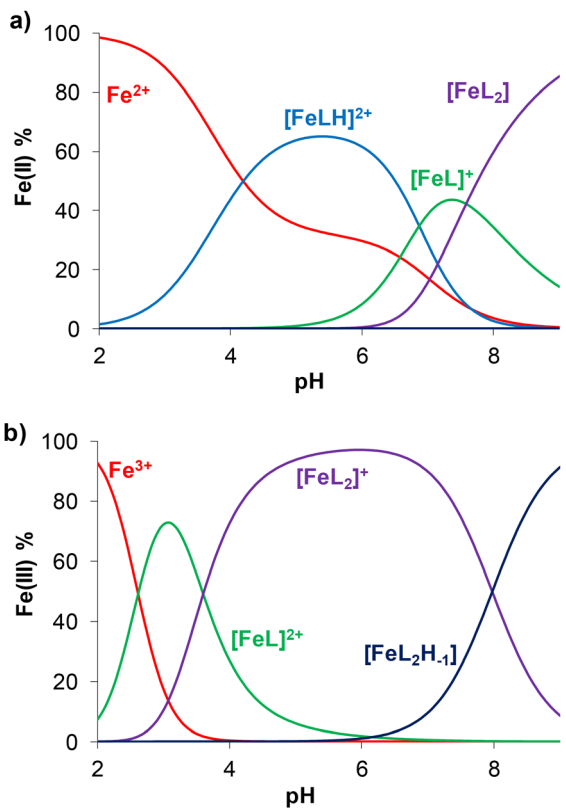

Fig. 7 Concentration distribution curves for the (a) Fe(II)–imidazole-TSC and (b) Fe(III)–imidazole-TSC systems {c_{lig} = 1 mM; $c_{Fe(II/III)}$ = 0.5 mM; T = 25.0 °C; I = 0.1 M (KCl)}.

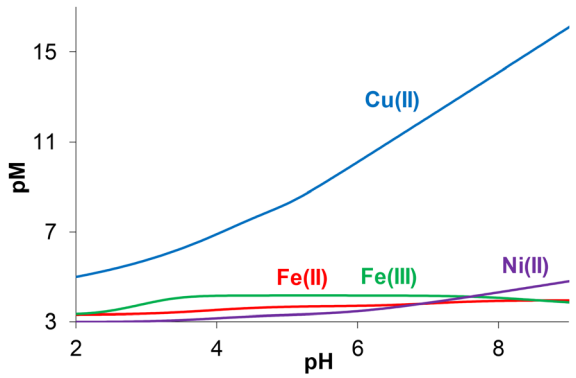

Fig. 8 Complex formation in the pH range 2–9 in 30% (v/v) DMSO/H_2O solvent mixture for the imidazole-TSC complexes of Cu(II) (blue solid line), Fe(III) (green solid line), Fe(II) (red solid line) and Ni(II) (violet solid line). {c_L = 1 mM; $c_{Fe(II)}$ = 1 mM, $c_{Fe(III)}$ = 1 mM, $c_{Ni(II)}$ = 1 mM, $c_{Cu(II)}$ = 1 mM; I = 0.1 M (KCl); T = 25 °C}.

Representative concentration distribution curves were calculated using the overall stability constants (Fig. 7), revealing that mono-ligand and protonated complexes are formed in the acidic pH range, whereas the bis-ligand $[Fe(III)L_2]^{+}$ and $[Fe(III)L_2H_{-1}]$ species predominate at pH > 5 for Fe(III) and $[Fe(II)L_2]$ for Fe(II) at pH > 7.

In order to compare the Cu(II), Ni(II), Fe(II) and Fe(III) binding abilities of the studied compound, pM values were calculated in the pH range 2–9 (Fig. 8) at equimolar ratio. Comparing these pM values of the imidazole-TSC complexes formed with Cu(II), Fe(II), Fe(III) and Ni(II) metal ions, it can be concluded that the ligand displays the strongest ability to form complexes with Cu(II), whereas lower pM values were obtained for Fe(II), Fe(III) and Ni(II) across the entire studied pH range.

2.5 Synthesis and characterization of Cu(II) complexes of imidazole-TSCs

Given the markedly high stability of the Cu(II) complexes in solution compared to the other metals, and the enhanced cytotoxic activity of the ligands observed upon complexation, we attempted to isolate the Cu(II) complexes for more detailed structural characterization in both solid and solution phases (Tables 1 and 3). Cu(II) complexes of imidazole-TSC derivatives were synthesized by reacting $CuCl_2$ with the corresponding ligand in a boiling mixture of MeOH/H_2O, affording yields of 69% to 84% (see Experimental).

The complexes were characterized using ESI-MS, UV-vis and EPR spectroscopy. In the ESI mass spectra recorded for metha-

nolic solutions, both dimeric and monomeric species were detected (Fig. S18–S21). However, the original protonation state of the complex cannot be determined by this method. The λ_{max} values of the complexes dissolved in methanol were observed at 284–298 nm and 338–342 nm for imidazole-TSC and its methylated derivatives, while somewhat higher values (316 nm and 407 nm) were obtained for benzimidazole-TSC. Comparison of these λ_{max} values and the corresponding spectra with those recorded for equimolar Cu(II) – ligand solutions in 30% (v/v) DMSO/H_2O at pH 4–5 (as shown in Fig. 3a for imidazole-TSC) indicates that the isolated complexes are mostly present in the $[CuL]^+$ form when dissolved in methanol. Accordingly, the solid-state complexes were identified as [CuLCl]. Notably, the same composition was found for the complexes of imidazole-TSC and imidazole-Me_2-TSC by SC-XRD (*vide infra*), although the single crystals were obtained from *in situ* prepared complexes. Isotropic EPR spectra of the Cu(II) complexes of imidazole-TSC, imidazole-Me-TSC and imidazole-Me_2-TSC complexes were recorded (Fig. 9), and no signals corresponding to free Cu(II) were detected; however, partial protonation of the complex was observed, which is likely caused by water traces in the samples. The spectra were well fitted by assuming a mixture of $[CuLH]^{2+}$ and $[CuL]^+$, with parameters summarized in Table S2. Methylation of the amine group did not induce any measurable change in the EPR parameters of the complexes, which remained identical within the standard deviations.

The stability of the Cu(II) complex of imidazole-TSC was further investigated by dissolving it in different solvents and biological media, including DMSO/MeOH, HEPES, Eagle's Minimal Essential Medium (EMEM), RPMI 1640 and human blood serum (HBS). As a comparison, $CuCl_2$ salt was also dissolved in the same medium without the ligand. The measured and simulated frozen solution EPR spectra are collected in Fig. S23 and the obtained simulation data are collected in Table S3.

In DMSO/MeOH the obtained simulation parameters closely match those determined for $[CuLH]^{2+}$ in prior pH-dependent EPR spectra analysis, suggesting that the complex existed predominantly in its protonated form under the conditions used. When the complex was dissolved in HEPES, RPMI 1640 or HBS, the spectrum remained characteristic of the complex (even after some min waiting time), with slightly shifts in parameters compared to DMSO due to solvent effects. Dissolving $CuCl_2$ salt in these media, Cu(II) was detected entirely (HEPES, RPMI 1640) or partially (HBS) in its low ligand field complex forms.

Ligand dissociation from this complex occurred exclusively in EMEM medium, as evidenced by the fact that the spectra of the complex and $CuCl_2$ salt were identical. This indicates that, in EMEM, the imidazole-TSC ligand was replaced by a more strongly binding ligand from the medium in the coordination sphere of Cu(II).

2.6 Structural characterization by single crystal X-ray crystallography

Single crystals suitable for SC-XRD measurements of the investigated ligands (except of benzimidazole-TSC) and their Cu(II) complexes could be obtained under crystallization conditions described in Section 4.4. The ORTEP representation of the obtained crystal structures of imidazole-TSC·H_2O (**I**), imidazole-Me-TSC (**II**), imidazole-Me_2-TSC (**III**) and imidazole-Me_2-TF·Cl (**IV**) are shown in Fig. 10. Packing of the molecules with the main hydrogen bond connections, asymmetrical units of selected crystals are shown in Fig. S24–S41. The hydrogen bond data, comparison of selected bond distances and angles are collected in Tables S4–S14.

Imidazole-TSC·H_2O (**I**) crystallized in the monoclinic crystal system in space group $P21/c$. The measurement was performed at 111 K. Previously this crystal was already measured at higher temperatures and the same form was found.[30,44] The perfectly planar molecules form chains and arranged in planes in the

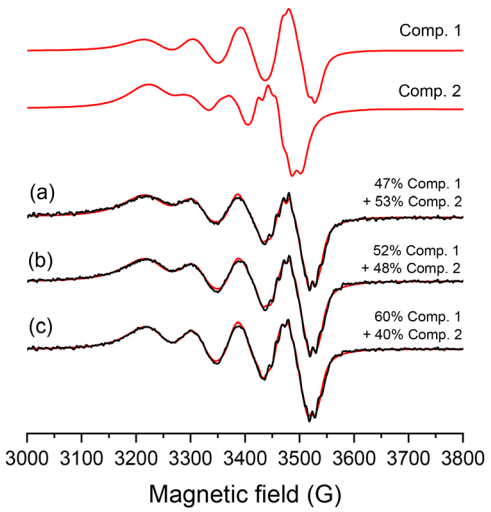

Fig. 9 Measured (black) and simulated (red) solution EPR spectra of complexes (a) Cu(II)–imidazole-TSC, (b) Cu(II)–imidazole-Me-TSC and (c) Cu(II)–imidazole-Me_2-TSC dissolved in DMSO at room temperature (298 K) with the ratio of the components (Comp. 1 as $[CuL]^+$ and Comp. 2 $[CuLH]^{2+}$). The obtained simulation data are collected in Table S2.

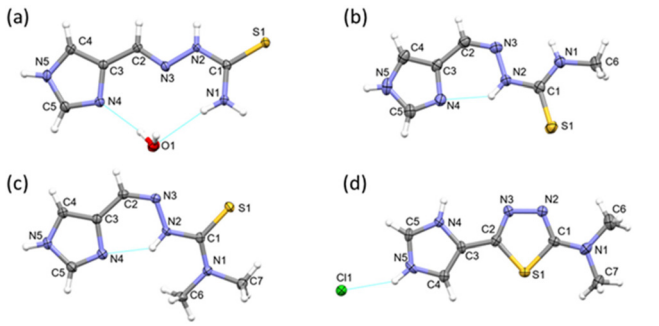

Fig. 10 ORTEP representation of crystal (a) imidazole-TSC·H_2O (**I**) (b) imidazole-Me-TSC (**II**) (c) imidazole-Me_2-TSC (**III**) and (d) imidazole-Me_2-TF × Cl (**IV**) with atom numbering. Displacement parameters are drawn at 50% probability level.

crystal, so water plays a major role in connecting the planes of the molecules through hydrogen bonds. One water molecule forms three hydrogen bonds with neighboring molecules.

The water oxygen and one of its hydrogen atoms are in H-bonds with the same imidazole-TSC molecule, bonding to the imidazole-N and amino hydrogen, respectively. The second water hydrogen is connected to the imidazole nitrogen of a neighboring molecule of an above plane. The imidazole-Me-TSC (**II**) crystallized in the orthorhombic crystal system in *Pbca* space group. An intramolecular hydrogen bond between imidazole-N and hydrazine-NH proton ensures the planar arrangement of the molecule in the crystal.

Hydrogen bonds play also a major role in stabilizing this crystal, but unlike imidazole-TSC, the molecules do not arrange in planes, they adopt a herringbone arrangement instead (see Fig. S26 and S27). This arrangement is due to the presence of the aminomethyl substituent as the CH_3 protons can form hydrogen bonds in three directions of space, resulting in a significantly different crystal structure compared to the planar parent compound.

The imidazole-Me_2-TSC (**III**) crystallized in the monoclinic crystal system in space group *P*21/*c*. The same intramolecular hydrogen bond detected in imidazole-Me-TSC ensures the planar conformation of this molecule as well (Fig. 10). The molecules are forming planes, similar to the imidazole-TSC crystal; however, the molecules in chain are not offset, but rotated 90 degrees one-by-one. Beside the hydrogen bond, offset parallel stacking interaction between imidazole rings (with distance between the two centers of gravities 3.763 Å) can play an important role in the stabilization of the crystal (Fig. S28 and S29). Selected hydrogen bond data are collected in Table S6. Interestingly, during the crystallization process of imidazole-Me_2-TSC in acidic conditions, a spontaneous cyclization resulted in the formation of 5-(1*H*-imidazole-4-yl)-*N*,*N*-dimethyl-2,5-dihydrothiophen-2-amine, which crystallized with a chloride counter ion (imidazole-Me_2-TF·Cl)(IV) in the orthorhombic crystal system, in space group *Cmc*21 (Fig. 10d and further information can be found in Fig. S30 and S31, Table S7). Spontaneous cyclization of TSCs was previously reported by Gričar *et al.*[45]

It is interesting to compare the conformation and bond length of the substituted imidazole-TSCs. Selected data are collected in Table S8. Notably, in the imidazole-TSC crystal, where the molecules are crystallized with a water, the TSC molecules adopt an (*E*) geometry. In contrast, in imidazole-Me-TSC and imidazole-Me_2-TSC crystals, where an intramolecular hydrogen bond of N2–H···N2 is present, the molecules adopted a (*Z*) geometry. Though both are (*Z*) isomers, the geometry of imidazole-Me-TSC and imidazole-Me_2-TSC also differs, as an additional 180° rotation occurs along the C1–N2 bond resulting in the torsion angle of N3–N2–C1–S1 177.72(12)° for imidazole-Me-TSC and 2.8(2)° for imidazole-Me_2-TSC. This may be related to the fact that an N1–H···N3 intramolecular H-bond can form in the case of imidazole-Me-TSC, whereas this is not possible in the case of the dimethyl derivative. Because of the electron-donating effect of the methyl substituents, we expected the C1–N1 bond to be shortest for the dimethyl derivative. Surprisingly, the opposite was measured due to the opposite steric effect of the bulky methyl groups. The length of the C1–S1 bond is equal within the standard deviation for all three compounds.

The Cu(II) complex of the imidazole-TSC crystallized in the monoclinic crystal system, in space group *C*2/*c* with a coordinated chloride ion, a NaCl salt, in the form of a hemihydrate with the composition [Cu(imidazole-TSCH$_{-1}$)Cl] × NaCl × 0.5H_2O (**V**). The ligand is negatively charged (L^-) in the complex since the hydrazine N2 nitrogen is deprotonated. The ORTEP representation of the coordination sphere of Cu(II) complex is shown in Fig. 11a. The ligand coordinates to Cu(II) as a tridentate ligand *via* ($N_{imdazile}$,N,S^-) donor set due to the tautomeric rearrangement. The complex adopts a square-planar coordination geometry. The deprotonated ligand also coordinates to a sodium ion. Four NaCl connect to two Cu(II) complex together in the crystal (Fig. S32 and S33). The neutral form of imidazole-Me-TSC crystallized with Cu(II) in the crystal [Cu(imidazole-Me-TSC)Cl_2] × 0.5H_2O (**VI**) (Fig. 11b) in the monoclinic crystal system, in *P*21/*c* space group. The ligand coordinates in a similar tridentate ($N_{imidazole}$,N,S) mode as in crystal (**V**) but the geometry is square pyramidal due to the presence of a second chloride in the apical position, which neutralizes the charge of the complex. There are two complexes and one water of crystallization in the asymmetrical unit of the crystal. The two complexes are almost identical, the planes of the ligands in the complexes are at an angle of 66.6° to each other (Fig. S34).

The ligand imidazole-Me_2-TSC crystallized with Cu(II) in its [Cu(imidazole-Me_2-TSCH$_{-1}$)Cl] × 1.5H_2O (**VII**) form in the *I*2/*a* space group in the monoclinic crystal system. The tridentate coordination of the deprotonated ligand and the square planar geometry with the coordination of one chlorido co-ligand in the fourth position makes it similar to crystal (**V**) (Fig. 11c).

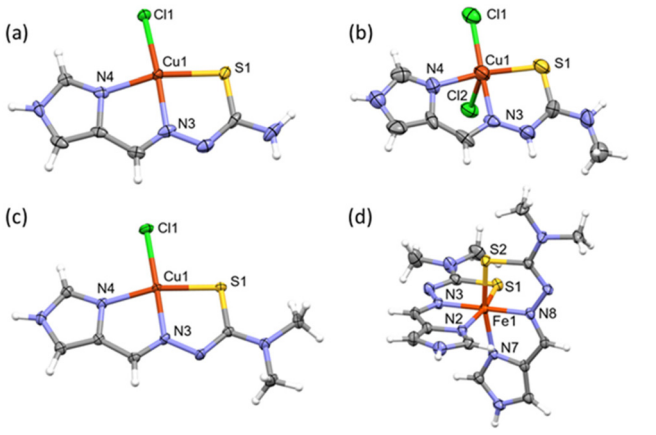

Fig. 11 ORTEP representation of crystals (a) [Cu(imidazole-TSCH$_{-1}$)Cl] × NaCl·H_2O (**V**) (b) [Cu(imidazole-Me-TSC)Cl_2] × 0.5H_2O (**VI**) (c) [Cu(imidazole-Me_2-TSCH$_{-1}$)Cl] × 1.5H_2O (**VII**) and (d) [Fe(imidazole-Me_2-TSCH$_{-1}$)$_2$] × Cl × MeOH (**VIII**) with atom numbering of the coordination sphere. Displacement parameters are drawn at 50% probability level.

Water of crystallization connects the complexes in the planes and between planes through N–H···O and O–H···Cl interactions (Fig. S37 and S38).

Based on the selected bond length and angles of the coordination sphere in crystals (**V**), (**VI**) and (**VII**) (Table S12), it can be concluded that the dimethylation of the amino group clearly results in a stronger binding of the ligand to Cu(II). The bond lengths between the metal ion and all the three coordinating donor atoms are significantly shortened in the dimethyl derivative compared to the parent compound, and the Cu1–Cl1 bond length increased. In crystal (**VI**), the coordination of the neutral ligand and an additional chlorido co-ligand in the apical position in complex [Cu(imidazole-Me-TSC)Cl_2] resulted in slightly longer Cu1–S1 and Cu1–N3 bonds compared to crystal (**V**) and (**VII**).

The Fe(III) complex of imidazole-Me_2-TSC could be crystallized in its [Fe(imidazole-Me_2-TSCH_{-1})$_2$]·Cl·MeOH form (Fig. 11d) in the monoclinic crystal system in *P*21/*c* space group containing two complexes with two chloride counter ions and two methanol solvates in the asymmetrical unit. The structure of the two complexes obtained in the asymmetrical unit is highly similar (Fig. S39), selected bond lengths are compared in Table S13. The geometry is octahedral around Fe(III), where both deprotonated ligand coordinates in the ($N_{imidazole}$, N,S^-) coordination mode. The complexes are connected through the chloride ions and methanol molecules creating H-bond interactions.

2.7 Redox properties of the Cu(II) complexes of imidazole-TSC derivatives

To investigate the redox properties of the isolated Cu(II) complexes, detailed electrochemical studies were performed using CV and UV-vis spectroelectrochemistry. Cyclic voltammograms of Cu(II) complexes of imidazole-TSCs were recorded in 99% (v/v) DMSO/H_2O using *n*-Bu_4NPF_6 as background electrolyte, in which all tested compounds exhibit good solubility. For comparison, the Cu(II)–triapine complex was also tested under identical conditions, having been prepared *in situ* by mixing $CuCl_2$ and the ligand in equimolar amounts. The cyclic voltammograms of all tested compounds are presented in Fig. 12 and the complexes show similar redox behavior. Namely, the electrochemical analysis reveals a single reduction peak accompanied by a strongly shifted re-oxidation peak.

These complexes showed very similar reduction peaks within the range from −0.1 to +0.1 V *vs.* NHE and a sharp oxidation peak appeared during the reverse scan in the range from +0.4 to +0.74 V *vs.* NHE. The electrochemical processes are electrochemically irreversible, however chemically reversible (only small changes in the shape of the cyclic voltammogram were observed upon redox cycling).

This behavior can be explained by an electrochemical dual-pathway square scheme (Scheme 3a), in which the electron transfer processes in Cu(II/I) systems are accompanied by substantial changes in coordination geometry.[46] Herein, Cu(II)L and Cu(I)L represent thermodynamically stable species with

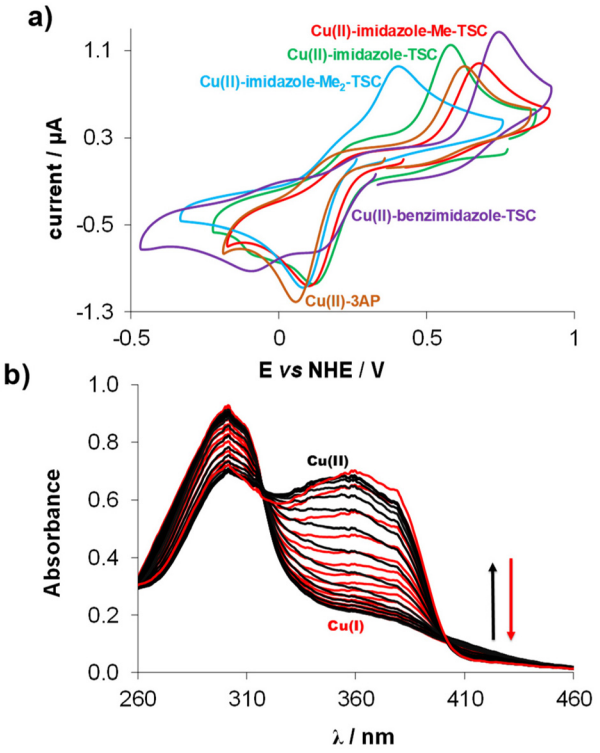

Fig. 12 (a) Cyclic voltammograms of the Cu(II)–TSC (1 : 1) systems in 99% (v/v) DMSO/H_2O at 100 mV s^{-1} scan rate {c_L = 1 mM, $c_{Cu(II)}$ = 1 mM, *T* = 25 °C, *I* = 0.1 M (*n*-Bu_4NPF_6)} *E′ vs.* NHE; (b) UV-vis spectra recorded for the Cu(II)–imidazole-Me_2-$_{TSC}$ (1 : 1) system at various potential values using the spectroelectrochemical cell. {$c_{Cu(II)}$ = c_L = 100 µM; *I* = 0.1 M (*n*-Bu_4PF_6); *T* = 25.0 °C, scan rate: 20 mV s^{-1}; ℓ = 0.17 cm}.

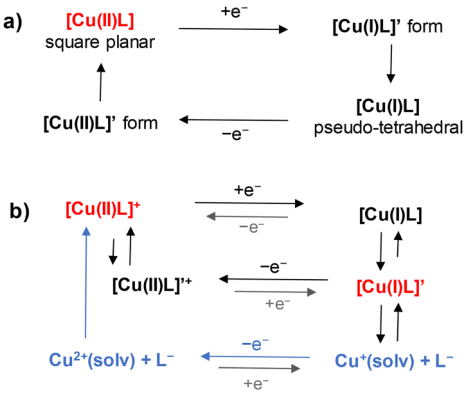

Scheme 3 Isomers (*Z*, major) and (*E*, minor) of imidazole-TSC in their H_2L^+, HL and L^- forms, where the suggested hydrogen bonds indicated with dashed lines based on Reference data.[34] Notably, the H_2L^+ form of the *E* isomer was not observed.

their characteristic coordination geometries (square-planar and pseudo-tetrahedral, respectively).

In contrast, Cu(II)L′ and Cu(I)L′ are metastable intermediates in which the coordination geometry nearly resembles that of the thermodynamically stable species of the opposite oxidation state (pseudo-tetrahedral and square-planar, respect-

ively). To gain a deeper understanding of these processes, UV-vis spectroelectrochemical measurements were performed, and the results for the Cu(II)–imidazole-Me$_2$-TSC system (1 : 1) are presented in Fig. 12b.

The UV-vis spectra of the initial complex show two absorption bands at 300 and 360 nm, with the former attributed to a ligand-centered transition and the latter assigned to an S → Cu charge transfer band. Upon reduction, a simultaneous decrease in the initial UV-vis absorption band at 360 nm and increase at 300 nm were observed, with an isosbestic point at 316 nm (Fig. 12b). The reoxidation process led to the complete restoration of the original absorption bands (Fig. 12b), confirming the sufficient stability of the generated Cu(I) complex of imidazole-Me$_2$-TSC and demonstrating the chemical reversibility of the redox cycling. Different behavior was found for the other compounds tested, where although an almost complete recovery of the initial optical bands of the original Cu(II) complex during back reoxidation was achieved, we indicated the release of the ligand upon the cathodic reduction. This corresponds well to the more complex reaction scheme (Scheme 3b), where during the back reoxidation of free solvated Cu(I) to Cu(II) state leads to the back formation of the stable initial Cu(II) complex.

Our findings are consistent with the results obtained from the direct reduction of other Cu(II)-TSC complexes with GSH. This reaction was monitored by UV-vis spectrophotometry under anaerobic conditions at pH 7.4 in aqueous solution. All Cu(II) complexes were rapidly reduced by GSH (<1 h), and the final spectrum corresponded to that of the free ligand (Fig. 13a).

Based on the spectral changes, the reaction rates of the tested Cu(II) complexes were found to be somewhat different (Fig. 13b), *e.g.* the benzimidazole-TSC complex reacted fastest, reaching equilibrium in less than 2 min. At the same time, the Cu(II) complex of imidazole-Me$_2$-TSC was reduced the most slower. The slower reaction with GSH was also found in our previous work for the dimethylated derivatives of triapine and FTSC.[35] Furthermore, introduction oxygen into the solutions of the reduced complexes regenerated the original complex, a phenomenon also observed in spectroelectrochemical studies (Fig. 12b).

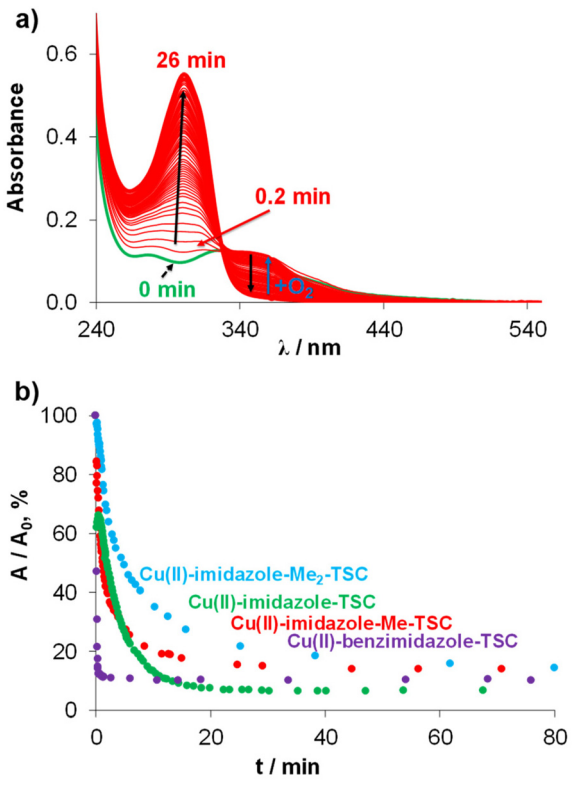

Fig. 13 (a) Time-dependent UV-visible absorption spectra of Cu(II)–imidazole-TSC (1 : 1) system in the presence of 50 equiv. GSH at pH = 7.4 (50 mM HEPES); {c_{Cu} = c_L = 25 μM; c_{GSH} = 1.25 mM; I = 0.1 M (KCl); ℓ = 1 cm; T = 25 °C}. (b) Absorbance values at 360 nm for Cu(II)–imidazole-TSC, for Cu(II)–imidazole-Me-TSC, for Cu(II)–imidazole-Me$_2$-TSC, at 416 nm for Cu(II)–benzimidazole-TSC systems with GSH in dependence of time. Absorbance value read from the first spectrum recorded after mixing of the reactants is considered as 100%.

3 Conclusions

To explore the impact of the ligand scaffold modification on the physico-chemical properties of TSCs, the α-*N*-pyridyl moiety was replaced with imidazole and benzimidazole units. Furthermore, the influence of various N-terminal substitutions, including methyl and dimethyl groups, was investigated. Such structural modifications are expected to improve the pharmacokinetic characteristics of TSCs by enhancing their solubility and bioavailability. The synthesis, characterization, and comparative study of the newly designed imidazole-derived TSCs with analogous reference compounds were carried out. For the ligands, two pK_a values were determined by pH-potentiometry. The lower one corresponds to the deprotonation of one of the imidazolium nitrogens (N3), while the higher one is associated with the hydrazonic nitrogen. The benzimidazole derivative has lower pK_a values than the imidazole analogue, which is attributed to the electron-withdrawing effect of the fused benzene ring. N-terminal monomethylation exerts little influence on proton dissociation, whereas dimethylation significantly lowers the pK_{a2} value. All the studied ligands are found in their neutral form at pH 7.4. Notably, imidazole-TSC exhibits slightly higher pK_a values than FTSC, the simplest α-*N*-pyridyl TSC. ^{1}H NMR spectroscopic titration of imidazole-TSC reveal that the (*Z*) isomer predominates in solution.

The interaction of imidazole-TSC derivatives with Fe(II), Fe(III), Cu(II), and Ni(II) was investigated using pH-potentiometry, UV-vis, and EPR (for Cu(II)) spectroscopic methods, and for Fe(II) complexes strictly anaerobic conditions were applied. The obtained solution equilibrium data indicates the formation of mono- and bis-ligand complexes of imidazole-TSCs with Fe(II) and Fe(III) ions. In the case of Ni(II), only mononuclear complexes are formed, whereas for Cu(II), in addition

to mono-ligand complexes, a tetrameric $[Cu_4L_4H_{-4}]$ species is also formed. EPR spectroscopic measurements confirmed the expected (N,N,S) coordination mode, which was further corroborated by SC-XRD analysis. Comparison of the solution stability of the imidazole-TSC complexes with different metal ions indicates that the ligands possess the greatest complex forming ability with Cu(II).

Electrochemical and spectroelectrochemical studies revealed that all Cu(II) complexes of imidazole-TSCs exhibit similar redox behavior, characterized by an irreversible Cu(II/I) redox couple with distinct reduction and oxidation peaks. The observed redox behavior is consistent with an electrochemical dual-pathway mechanism involving geometry changes between square-planar and pseudo-tetrahedral configurations of the Cu(II) and Cu(I) complexes, respectively, slowing down the electron-transfer kinetics and resulting in electrochemical irreversibility. UV-vis spectroelectrochemistry was used to confirm the reversible transformation and the high stability of the Cu(I) species, particularly for the imidazole-Me_2-TSC complex. Furthermore, reduction experiments with GSH demonstrated comparable reactivity among the complexes, with benzimidazole-TSC showing the fastest reduction and oxygen-dependent reoxidation, thus supporting the chemical reversibility of these systems.

The cytotoxic activity of imidazole-TSC derivatives was tested against human cancer cell lines such as chemosensitive Colo205 and doxorubicin-resistant Colo320. The imidazole-TSC derivatives exhibited varying anticancer activities, which were significantly enhanced upon coordination with Cu(II) or Ni(II) ions. Among the free ligands, imidazole-Me_2-TSC showed the strongest cytotoxicity against both Colo205 and Colo320 cancer cells, although it is less cytotoxic than the corresponding α-*N*-pyridyl TSCs, such as triapine. Notably, this compound exhibited a degree of selectivity toward these cancer cell lines compared to non-cancerous fibroblasts. Upon complexation with Cu(II), its activity remained in the low μM range, although it was not further enhanced. Comparison of imidazole-Me_2-TSC with the non- and mono-substituted derivatives reveals that it exhibits a lower pK_{a2} value and slightly increased lipophilicity. While their Cu(II) complexes have similar thermodynamic stability, the Cu(II) complex of imidazole-Me_2-TSC is reduced more slowly by GSH, which may contribute to its pronounced biological activity. Benzimidazole-TSC was practically inactive, which may be attributed to its very poor aqueous solubility, likely limiting its cellular uptake. In contrast, metal coordination significantly improved its cytotoxicity, despite the lower complex stability and the rapid reaction of the Cu(II) complex with GSH, suggesting an improve cellular uptake due to the complex formation.

4 Materials and methods

4.1 Chemicals

For the synthesis of TSC ligands, all reagents and solvents were obtained from commercial suppliers (Sigma-Aldrich and TCI) and used as received. KCl, KOH, HCl, DMSO were obtained from Reanal (Hungary), 4-(2-hydroxyethyl)-1-piperazineethane-sulfonic acid (HEPES) were purchased from Sigma-Aldrich and used without further purification. $CuCl_2$, $FeCl_3$ and $NiCl_2$ Reanal (Hungary) were dissolved in a known amount of HCl to obtain the Cu(II), Fe(III) and Ni(II) stock solutions, respectively. Their concentrations were determined by complexometry through the ethylenediaminetetraacetate (EDTA) complexes. The Fe(II) stock solution was obtained from fine iron powder dissolved in a known amount of HCl solution under a purified, strictly oxygen-free argon atmosphere, then filtered, stored and used under anaerobic conditions in a laboratory glove box (GP(Campus) Jacomex, O_2 content ≤1 ppm). KSCN solution was used to check the absence of Fe(III) traces in the Fe(II) solution. The concentration of the Fe(II) stock solution was determined by permanganometric titrations under acidic conditions. Accurate strong acid content of the metal stock solutions was determined by pH-potentiometric titrations. The ligand stock solutions were prepared on a weight-in-volume basis dissolved in DMSO. Reagents and materials used for the synthesis were purchased from Alfa Aesar. All solvents were dried and purified according to standard procedures.

Melting points (Mp) were determined on an SRS Optimelt digital apparatus and are uncorrected. For MW-assisted syntheses, a CEM Discover SP laboratory MW reactor was used with a max. power of 200 W (running a dynamic control program). The transformations were monitored by TLC using 0.25 mm thick Kieselgel-G plates (Si 254 F, Merck). The compound spots were detected under UV light (λ = 254 nm). Flash chromatographic purifications were carried out on silica gel 60, 40–63 μm (Merck) using different solvent systems (ss), like MeOH/EtOAc = 5 : 95 (ss A), 10 : 90 (ss B) or 20 : 80 (ss C) or pure EtOAc (ss D). NMR spectra were recorded with a Bruker DRX 500 instrument at room temperature in DMSO-d_6 using residual solvent signal as an internal reference. Chemical shifts are reported in ppm (δ scale), and coupling constants (J) are given in Hz. Multiplicities of the ^{1}H signals are indicated as a singlet (s), a broad singlet (bs), a doublet (d) or a multiplet (m). ^{13}C NMR spectra are ^{1}H-decoupled and the J-MOD pulse sequence was used for multiplicity editing. In this spin-echo type experiment, CH_3 and CH carbons appear as positive signals, while CH_2 and C carbons as negative signals.

A Waters Q-TOF Premier (Micromass MS Technologies) mass spectrometer with an electrospray ion source was used to perform high-resolution (HR) ESI-MS experiments. Samples contained 100 μM compounds in methanol (LC-MS grade).

4.2 Synthesis of TSC ligands

General procedure for the synthesis of imidazole thiosemicarbazones. Method A. 1*H*-Imidazole-4-carbaldehyde (1, 480 mg, 5 mmol) and the appropriate thiosemicarbazide derivative (1 equiv.) were reacted in absolute EtOH (25 mL) containing a catalytic amount of glacial acetic acid (AcOH, 0.2 mL), and the mixture was kept at reflux temperature for 5 h. After completion of the reaction (determined by TLC), most of the EtOH was evaporated *in vacuo* and the resulting

crystals were cooled, filtered off and recrystallized from MeOH/H_2O = 1 : 1 to afford the corresponding product.

Method B. The mixture of 1*H*-imidazole-4-carbaldehyde (1, 192 mg, 2 mmol), the appropriate thiosemicarbazide derivative (1.2 equiv.) and glacial acetic acid (AcOH, 0.1 mL) in EtOH (5 mL) was irradiated by microwave (MW) at 90 °C for 15 min. After completion of the reaction (determined by TLC), the solution was poured into water and the precipitate was filtered off. The crude product was purified by column chromatography.

2-((1H-Imidazol-4-yl)methylene)hydrazine-1-carbothioamide (imidazole-TSC). According to the general procedure, thiosemicarbazide (456 mg, Method A or 219 mg, Method B) was used for the syntheses to afford the product as a brownish solid. Yield: 618 mg (73%, Method A) or 291 mg (86%, Method B, ss A). Mp. 200–202 °C (201–202 °C;[30]) ^{1}H NMR (500 MHz, DMSO-d_6): δ (*E*/*Z* isomers): 7.22 (s, 1H, 2-H, *E*), 7.41 (bs, 1H, 5-H, *Z*), 7.69 (s, 1H, 5-H, *E*), 7.79 (s, 1H, CH═N, *Z*), 7.80 (s, 1H, one of NH_2, *E* and *Z*), 7.95 (s, 1H, 2-H, *Z*), 8.03 (s 1H, CH═N, *E*), 8.13 (bs, 1H, the other of NH_2, *Z*), 8.20 (bs, 1H, the other of NH_2, *E*), 11.35 (s, 1H, chain-NH, *Z*), 12.45 (bs, 1H, imidazole-NH, *Z*), 12.80 (bs, 1H, imidazole-NH, *E*), 13.03 (s, chain-NH, *E*) ppm; ^{13}C NMR (125 MHz, DMSO-d_6): δ (*E*/*Z* configuration): 121.5 (C-5), 131.0 (C-2), 135.5 (C-4), 136.5 (CH═N, *Z*) and 137.3 (CH═N, *E*), 177.6 (C═S, *Z*), 177.9 (C═S, *E*) ppm; HR-ESI-MS (ESI+) (*m*/*z*): calcd: $C_5H_5N_4S$ $[M + H - NH_3]^+$ = 153.0229 found 153.0079, $C_5H_8N_5S$ $[M + H]^+$ = 170.0495 found 170.0439, $C_5H_6N_5SFe$ $[M - H + Fe]^+$ = 223.9693 found 223.9626, $C_{10}H_{12}N_{10}S_2Fe$ $[2M - 2H + Fe]^+$ = 392.0048 found 391.9937. λ_{max} in MeOH: 308 nm.

2-((1H-Imidazol-4-yl)methylene)-N-methylhydrazine-1-carbothioamide (imidazole-Me-TSC). According to the general procedure 4-methyl-3-thiosemicarbazide (526 mg, Method A or 252 mg, Method B) was used for the syntheses to afford the product as a beige solid. Yield: 724 mg (79%, Method A) or 319 mg (87%, Method B, ss B). Mp. 192–194 °C; ^{1}H NMR (500 MHz, DMSO-d_6): δ (*E*/*Z* isomers): 2.98 (d, 3H, *J* = 4.6 Hz, N–CH_3, *E*), 3.02 (d, 3H, *J* = 4.6 Hz, N–CH_3, Z), 7.21 (s, 1H, 2-H, *E*), 7.42 (bs, 1H, 5-H, *Z*), 7.68 (s, 1H, 5-H, *E*), 7.79 (s, 1H, CH═N, *Z*), 7.96 (s, 1H, 2-H, *Z*), 8.03 (s 1H, CH═N, *E*), 8.31 (bs, 1H, N–CH_3, *Z*), 8.48 (d, 1H, *J* = 4.6 Hz, N–CH_3, *E*), 11.36 (s, 1H, chain-NH, *Z*), 12.40 (bs, 1H, imidazole-NH, *Z*), 12.80 (bs, 1H, imidazole-NH, *E*), 13.06 (s, chain-NH, *E*) ppm; ^{13}C NMR (125 MHz, DMSO-d_6): δ (*E*/*Z* configuration): 30.5 (N–CH_3, *Z*), 30.8 (N–CH_3, *E*), 121.3 (C-5), 130.4 (C-2), 135.5 (C-4), 136.5 (CH═N), 177.5 (C═S, *Z*), 177.7 (C═S, *E*) ppm; HR-ESI-MS (ESI+) (*m*/*z*): calcd: $C_6H_{10}N_5S$ $[M + H]^+$ = 184.0651 found 184.0596, $C_6H_8N_5SFe$ $[M - H + Fe]^+$ = 237.9850 found 237.9781, $C_{12}H_{16}N_{10}S_2Fe$ $[2M - 2H + Fe]^+$ = 420.0350 found 420.0226. λ_{max} in MeOH: 308 nm.

2-((1H-Imidazol-4-yl)methylene)-N,N-dimethylhydrazine-1-carbothioamide (imidazole-Me$_2$-TSC). According to the general procedure 4,4-dimethyl-3-thiosemicarbazide (596 mg, Method A or 286 mg, Method B) was used for the syntheses to afford the product as a beige solid. Yield: 641 mg (65%, Method A) or 343 mg (87%, Method B, ss C). Mp. 208–210 °C; ^{1}H NMR (500 MHz, DMSO-d_6): δ (*E*/*Z* isomers): 2.26 (s, 6H, 2 × N–CH_3, *Z*), 3.32 (s, 6H, 2 × N–CH_3, *E*), 7.37 (s, 1H, 2-H, *E*), 7.67 (s, 1H, 5-H, *E*), 8.03 (s 1H, CH═N, *E*), 12.81 (bs, 1H, imidazole-NH, *E*), 13.62 (s, chain-NH, *E*) ppm; ^{13}C NMR (125 MHz, DMSO-d_6): δ (*E*/*Z* configuration): 40.9 (2 × N–CH_3, *E*), 42.2 (2 × N–CH_3, *Z*), 120.3 (C-5, *E*), 132.9 (C-2, *E*), 135.6 (C-4, *E*), 136.1 (CH═N, *E*), 179.8 (C═S, *E*) ppm; HR-ESI-MS (ESI+) (*m*/*z*): calcd: $C_7H_{10}N_5SFe$ $[M - H + Fe]^+$ = 252.0006 found 251.9931, $C_{14}H_{20}N_{10}S_2Fe$ $[2M - 2H + Fe]^+$ = 448.0663 found 448.0569. λ_{max} in MeOH: 296 nm.

2-((1H-Benzimidazol-2-yl)methylene)hydrazine-1-carbothioamide (benzimidazole-TSC). 1*H*-Benzimidazole-2-carbaldehyde (292 mg, 2 mmol) and thiosemicarbazide (219 mg, 1.2 equiv.) were reacted in EtOH (20 mL) and water (5 mL) containing a catalytic amount of glacial acetic acid (AcOH, 0.1 mL), and the mixture was kept at reflux temperature for 24 h. After completion of the reaction (determined by TLC), most of the EtOH was evaporated *in vacuo* and the resulting crystals were cooled, filtered off and dried. The crude product was purified by column chromatography (ss D). Yellow solid. Yield: 276 mg (63%). Mp. 215 °C (decomp); ^{1}H NMR (500 MHz, DMSO-d_6): δ 7.19 (t-like m, 1H) and 7.27 (t-like m, 1H, 5-H and 6-H), 7.51 (d, 1H, *J* = 8.0 Hz) and 7.64 (d, 1H, *J* = 8.0 Hz, 4-H and 7-H), 8.03 (s, 1H, 8-H) 8.29 (s, 1H, one of NH_2), 8.55 (s, 1H, the other of NH_2), 11.84 (s, 1H, 9-H), 12.69 (s, 1H, 1-H) ppm; ^{13}C NMR (125 MHz, DMSO-d_6): 111.2 (C-7), 119.4 (C-4), 121.8 (C-5), 123.8 (C-6), 131.6 (C-8), 134.0 (C-7a), 143.8 (C-3a), 148.7 (C-2), 178.6 (C-10) ppm; HR-ESI-MS (ESI+) (*m*/*z*): calcd: $C_9H_7N_4S$ $[M + H - NH_3]^+$ = 203.0386 found 203.0333, $C_{18}H_{16}N_{10}S_2Fe$ $[2M - 2H + Fe]^+$ = 492.0386 found 492.0222. λ_{max} in MeOH: 342 nm.

4.3 Synthesis and characterization of the Cu(II) complexes

Imidazole and benzimidazole thiosemicarbazone Cu(II) complexes were obtained in a good yield (up to 84%) after the reaction between the corresponding TSC (1 equiv.) and $CuCl_2 \times 2$ H_2O (1 equiv.) in the presence of triethylamine (Et_3N) (1 equiv.). Afterwards, the solution was allowed to stand in an open beaker at room temperature. The green crystalline product was filtered off, washed with Et_2O (5–10 mL) and dried in air. The solid complexes were characterized by ESI-MS, UV-vis and EPR spectroscopy.

Cu(II)–imidazole-TSC. Yield: 69%; ESI-MS (MeOH, positive): *m*/*z* 230.9635, 230.9639 calcd for $[C_5H_6CuN_5S]^+$; *m*/*z* 498.8938, 498.8950 calcd for $[C_{10}H_{12}Cu_2N_{10}S_2]Cl$; λ_{max} in MeOH: 284, 338 nm.

Cu(II)–imidazole-Me-TSC. Yield: 74%; ESI-MS (MeOH, positive): *m*/*z* 244.9786, 244.9796 calcd for $[C_6H_8CuN_5S]^+$; *m*/*z* 526.9239, 526.9263 calcd for $[C_{12}H_{16}Cu_2N_{10}S_2]Cl$; λ_{max} in MeOH: 294, 334 nm.

Cu(II)–imidazole-Me$_2$-TSC. Yield: 81%; ESI-MS (MeOH, positive): *m*/*z* 258.9948, 258.9952 calcd for $[C_7H_{10}CuN_5S]^+$; *m*/*z* 554.9562, 554.9576 calcd for $[C_{14}H_{20}Cu_2N_{10}S_2]Cl$; λ_{max} in MeOH: 298, 342 nm.

Cu(II)–benzimidazole-TSC. Yield: 84%; ESI-MS (MeOH, positive): *m*/*z* 280.9794, 280.9796 calcd for $[C_9H_8CuN_5S]^+$; *m*/*z* 598.9256, 598.9263 calcd for $[C_{18}H_{16}Cu_2N_{10}S_2]Cl$; λ_{max} in MeOH: 316, 407 nm.

4.4 Crystallization procedure, single crystal X-ray data collection, structure solution and refinement

Colorless needle shape crystal of imidazole-TSC·H_2O (**I**) suitable for SC-XRD analysis was obtained by slow evaporation from THF/MeOH solution mixture. Colorless block crystals of imidazole-Me-TSC (**II**) and imidazole-Me_2-TSC (**III**) were obtained from MeOH/water and THF/MeOH solvent mixtures, respectively. During the crystallization process of imidazole-Me_2-TSC in acidic conditions, a spontaneous cyclisation reaction resulted in the formation of 5-(1*H*-imidazole-4-yl)-*N*,*N*-dimethyl-2,5-dihydrothiophen-2-amine which crystallized with a chloride counter ion (imidazole-Me_2-TF·Cl) (**IV**)). These colorless needle crystals were crystallized from the ethanolic solutions of the compounds. The single crystals of the Cu(II) complexes were obtained from equimolar methanolic solution of the ligand and $CuCl_2$. To ensure complete deprotonation of the ligand during complex formation, an equimolar amount of sodium methoxide was added yielding complexes with the deprotonated ligand form. Green prism crystal of [Cu(imidazole-TSCH_{-1})Cl]·NaCl·H_2O (**V**) was obtained from MeOH by vapor diffusion with diethyl ether. Brown platelet crystal of [Cu(imidazole-Me_2-TSCH_{-1})Cl] × 1.5H_2O (**VII**) was crystallized from MeOH by vapor diffusion with diethyl ether. However, in the case of imidazole-Me-TSC, the addition of base did not lead to crystallization of the deprotonated complex. Single crystals were obtained only from experiments performed without base, affording green rhombohedral shaped crystals of [Cu(imidazole-Me-TSC)Cl_2] × 0.5H_2O (**VI**), in which the ligand remains in its neutral form. Green platelet crystal of [Fe(imidazole-Me_2-TSCH_{-1})$_2$]Cl × MeOH (**VIII**) which was prepared by mixing imidazole-Me_2-TSC with $FeCl_3$ and sodium methoxide in a 2 : 1 : 2 ratio in MeOH. The growth of the crystal was achieved by slow solvent evaporation.

All X-ray diffraction data were collected on a Rigaku RAXIS-RAPID II diffractometer using Mo-Kα radiation. The measuring temperatures were 111 K, 153 K, 103 K and 125 K in case of crystals **I**, **II**, **III** and **IV** respectively. For complex crystals **V**, **VI**, **VII** and **VIII** measuring temperatures of 113 K, 103 K, 120 K and 103 K were used, respectively. Numerical absorption correction was carried out using the program CrystalClear.[47] Using Olex2,[48] the structure was solved with the SHELXT[49] structure solution program using Intrinsic Phasing and refined with the olex2.refine[50] refinement package using Gauss–Newton minimization. Refinement of non-hydrogen atoms was carried out with anisotropic temperature factors. Hydrogen atoms were placed into geometric positions. They were included in structure factor calculations but they were not refined. The isotropic displacement parameters of the hydrogen atoms were approximated from the U(eq) value of the atom they were bonded to. The summary of data collection and refinement parameters are collected in Tables S15 and S16. Graphical representation and the edition of CIF files were done by Mercury[51] and enCIFer[52] softwares. CCDC 2512498–2512505 contain the supplementary crystallographic data for this contribution.

4.5 Lipophilicity and solubility at pH 7.4

Distribution coefficient ($D_{7.4}$) values of the ligands were determined by the shake-flask method in *n*-octanol/buffered aqueous solution at pH 7.4 in 20 mM phosphate buffer (0.10 M KCl) at 25.0 ± 0.2 °C following a similar approach to that reported in our previous works.[53] The other compounds and all of their Cu(II) complexes were too lipophilic to obtain experimental data.

The thermodynamic solubility of the ligands was measured for the saturated solutions in water at pH 7.4 (20 mM HEPES buffer) at 25.0 ± 0.1 °C. The concentrations of the compounds were determined by UV-vis spectrophotometry using stock solutions of the compounds with known concentrations dissolved in pure DMSO, and 50% and 1% (v/v) DMSO/buffered aqueous solution for the calibration.

4.6 Solution equilibrium studies: pH-potentiometry

pH-potentiometry was applied for the determination of the proton dissociation constants (pK_a) of imidazole-TSC, imidazole-Me-TSC, imidazole-Me_2-TSC, benzimidazole-TSC and for the calibration of the electrode system used for the UV-vis and ^{1}H NMR titrations as well. Furthermore, pH-potentiometry was applied to determine the overall stability constants of the imidazole-TSC complexes with Fe(II), Fe(III) and Ni(II) ions. The measurements were performed in water using 0.10 M KCl background electrolyte at 25.0 ± 0.1 °C as described in our previous works.[34,41] For the titrations, an Orion 710 A pH-meter equipped with a Metrohm combined electrode (type 6.0234.100) and a Metrohm 665 Dosimat burette were used. The electrode system was calibrated to the pH = $-\log[H^+]$ scale by the method suggested by Irving *et al.*[54] The obtained average water ionization constant (pK_w) was 14.53 ± 0.05, which corresponds well to literature data.[34,41] Samples were deoxygenated by bubbling purified argon through them for *ca.* 10 min prior the measurements. In the case of Fe(II) samples, argon over-pressure was used when Fe(II) was added to the samples in tightly closed vessels, which were completely deoxygenated by bubbling a stream of purified argon through them for approximately 20 min prior to work up. Argon was also passed over the solutions during the titrations.

The calculations were always made from the experimental titration data measured in the absence of any precipitate in the solution. For the determination of the pK_a values of imidazole-TSC, imidazole-Me-TSC, imidazole-Me_2-TSC and benzimidazole-TSC the initial volume of the samples was 10.0 mL in which the ligand concentration was 1–2 mM. The pH-potentiometric titrations were performed in the pH range 2.0–12.5 and metal-to-ligand ratios of 1 : 1–1 : 4 were used. The proton dissociation constants of the ligands, the stoichiometry and overall stability constants of the complexes were determined with the computer program Hyperquad[55] ($\beta(M_pL_qH_r)$). $\beta(M_pL_qH_r)$ is defined for the general equilibrium pM + qL + rH $\rightleftharpoons$ $M_pL_qH_r$ as $\beta(M_pL_qH_r) = [M_pL_qH_r]/[M]^p[L]^q[H]^r$, where M denotes the metal ion and L the completely deprotonated ligand.

4.7 Solution phase spectroscopic studies: UV-visible spectrophotometry, EPR and ^{1}H NMR spectroscopy

An Agilent Cary 8454 diode array spectrophotometer was used to record the UV-vis spectra at an interval of 200–800 nm. The path length was 0.5–2 cm. Spectrophotometric titrations were performed using a 0.1 M KOH titrant solution with 30% (v/v) DMSO on samples with 30% (v/v) DMSO containing HCl, KCl and the ligand at 20–117 μM concentration in the pH range 2.0–12.5 in the presence of 1 or 0.5 equiv. Cu(II) ions. The overall stability constants (β) of the Cu(II) complexes and the UV-vis spectra of the individual species were calculated by the computer program PSEQUAD[56] as was done in our previous works.[34,53]

The redox reaction of the Cu(II) complexes with GSH was studied at 25.0 ± 0.1 °C, at pH 7.40 (10 mM HEPES with 0.1 M KCl) on an Agilent Cary 8454 diode array spectrophotometer using a special, tightly closed tandem cuvette (Hellma Tandem Cell, 238-QS). The complex and the reducing agent were separated until the reaction was triggered. Both isolated pockets of the tandem cuvette were completely deoxygenated by bubbling argon for 10 min before mixing the reactants. Spectra were recorded before and then immediately after the mixing, and changes were followed till no further absorbance change was observed.

The ^{1}H NMR spectra at different pH values were recorded using a Bruker Avance III HD Ascend 500 Plus instrument (with DSS as an internal reference). Water suppression was applied with a pulse sequence called WATERGATE. For titrations, the samples contained 3 mM imidazole-TSC, 30% (v/v) DMSO/H_2O and 0.10 M KCl.

All CW-EPR spectra were recorded with a BRUKER EleXsys E500 spectrometer (microwave frequency 9.43 GHz, microwave power 13 mW, modulation amplitude 5 G, modulation frequency 100 kHz). Two series of pH-dependent EPR spectra were recorded, one at equimolar Cu(II) and imidazole-TSC (c_{Cu} = 0.6 mM) and another at two-fold ligand excess at 0.25 mM Cu(II) and 0.5 mM ligand concentration in 30% (v/v) DMSO/H_2O. The powder of the isolated Cu(II)–imidazole-TSC, imidazole-Me-TSC and imidazole-Me_2-TSC complexes were dissolved in pure DMSO (at 3 mM concentration) and measured in capillaries at room temperature. EPR spectra of $CuCl_2$ and Cu-imidazole-TSC powder after dissolution in different solvents and biological media (DMSO/MeOH, HEPES, EMEM, RPMI 160 and blood serum medium) in 1–2 mM concentration were measured in frozen solution (77 K). For the low temperature measurements 0.2 mL samples were taken into quartz EPR tubes (0.05 ml MeOH was added to avoid water crystallization upon freezing) and measured in a dewar containing liquid nitrogen (77 K).

All EPR spectra were simulated by a designated software written by Rockenbauer and Korecz.[57] Rhombic or axial g-tensor (with main values g_x, g_y, g_z) and A-tensor (with main values A_x, A_y, A_z) and in case of resolved nitrogen splitting rhombic nitrogen hyperfine tensor (a_x^N, a_y^N, a_z^N where x, y and z denotes the directions of the g-tensor) were fitted. For the description of the linewidth the orientation dependent α, β and γ parameters were used to set up each component spectra, where α, β, and γ defined the linewidths through the equation $\sigma m_I = \alpha + \beta m_I + \gamma m_I^2$, where m_I denotes the nuclear magnetic quantum number of Cu(II) (I_{Cu} = 3/2). Since a natural Cu(II) chloride was used for the measurements, both the isotropic and anisotropic spectra were calculated as the sum of the spectra of ^{63}Cu and ^{65}Cu weighted by their natural abundances.

4.8 Electrochemical and spectroelectrochemical studies

Cyclic voltammetric experiments for the Cu(II) and Fe(III) complexes of imidazole-TSC, imidazole-Me-TSC, imidazole-Me_2-TSC and benzimidazole-TSC (c = 0.1 mM) in DMSO (SeccoSolv max. 0.025% H_2O, Merck) using n-Bu_4NPF_6 (*puriss* quality from Fluka, c = 0.1 M) as supporting electrolyte were performed under argon atmosphere using a three electrode arrangement with glassy-carbon 1 mm disc working electrodes (Ionode), platinum wire as counter electrode, and silver wire as pseudo-reference electrode. Ferrocene (Sigma-Aldrich) served as the internal potential standard for non-aqueous systems. A Heka PG310USB (Lambrecht, Germany) potentiostat with a PotMaster 2.73 software package served for the potential control in voltammetric studies. *In situ* ultraviolet-visible-near-infrared (UV/Vis/NIR) spectroelectrochemical measurements were performed on a spectrometer (Avantes, Model AvaSpec-2048 × 14-USB2) in the spectroelectrochemical cell kit (AKSTCKIT3) with the Pt-microstructured honeycomb working electrode, purchased from Pine Research Instrumentation (Lyon, France). The cell was positioned in the CUV-UV Cuvette Holder (Ocean Optics, Ostfildern, Germany) connected to the diode-array UV/Vis/NIR spectrometer by optical fibers. UV/Vis/NIR spectra were processed using the AvaSoft 7.7 software package. Halogen and deuterium lamps were used as light sources (Avantes, Model AvaLight-DH-S-BAL).

4.9 Cell lines and culture conditions and *in vitro* cytotoxicity assay

Two cancer cell lines have been used in this study: the doxorubicin-sensitive Colo205 (CCL-222, ATCC, Manassas, VA, USA) human colonic adenocarcinoma cell line and the doxorubicin-resistant Colo320/MDR-LRP expressing P-glycoprotein (P-gp, ABCB1) (MDR1)-LRP (CCL-220.1, ATCC) human colonic adenocarcinoma cell line (LGC Promochem, Teddington, UK). MRC-5 human embryonal lung fibroblast cell line was purchased from LGC Promochem. The Colo205 and Colo320 cell lines were cultured in RPMI 1640 medium supplemented with 10% fetal bovine serum (FBS), 2 mM L-glutamine, 1 mM Na-pyruvate and 10 mM HEPES. The MRC-5 cells were cultured in EMEM supplemented with a non-essential amino acid mixture, a selection of vitamins, 10% heat-inactivated fetal bovine serum, 2 mM L-glutamine, 1 mM sodium pyruvate. All cell lines were incubated at 37 °C, 5% CO_2, 95% air atmosphere. The cells were detached with Trypsin-Versene (EDTA) solution for 5 min at 37 °C.

The tested compounds were dissolved in 90% (v/v) DMSO/H_2O at 10 mM concentration. The complexes were prepared *in situ*, namely, equimolar solutions of the ligand (imidazole-TSC, imidazole-Me-TSC, imidazole-Me_2-TSC and benzimidazole-TSC) and the divalent metal ion salt ($CuCl_2$ and $NiCl_2$) were used for the biological assays. The metal salts without ligands were also tested. Doxorubicin (Merck) was used as a positive control. The stock solutions were diluted in RPMI 1640/EMEM culture medium, and two-fold serial dilutions of compounds were prepared horizontally in 100 μL of RPMI 1640/EMEM medium. The final concentration of DMSO in the medium did not exceed 1% (v/v) at which cell viability was not inhibited. All cancer cells were treated with Trypsin-Versene (EDTA) solution. The colon adenocarcinoma cells were adjusted to a density of 1×10^4 cells in 100 μL of RPMI 1640 medium, and were added to each well, with the exception of the medium control wells. The final volume of the wells containing compounds and cells was 200 μL. The culture plates containing the cells were incubated at 37 °C for 72 h; and at the end of the incubation period, 20 μL of 3-(4,5-dimethylthiazol-2-yl)-2,5-diphenyltetrazolium bromide (MTT) solution (from a stock solution of 5 mg mL^{-1}) were added to each well. After incubation at 37 °C for 4 h, 100 μL of sodium dodecyl sulphate (SDS) solution (10% in 0.01 M HCl) were added and the plates were further incubated at 37 °C overnight. The cell growth was determined by measuring the optical density (OD) at 450 nm (ref. 620 nm) with a Multiscan EX ELISA reader. Inhibition of the cell growth (expressed as IC_{50}: inhibitory concentration that reduces by 50% the growth of the cells exposed to the tested compounds) was determined from the sigmoid curve, where $100 - ((OD_{sample} - OD_{medium\ control})/(OD_{cell\ control} - OD_{medium\ control})) \times 100$ values were plotted against the logarithm of compound concentrations. Curves were fitted by GraphPad Prism software[58] using the sigmoidal dose–response model (comparing variable and fixed slopes). The IC_{50} values were obtained from at least 3 independent experiments.

4.10 Bacterial cell culture and MIC determination

Escherichia coli ATCC 25922 and *Klebsiella quasipneumoniae* ATCC 700603 Gram-negative strains were studied in the experiments. Methicillin-resistant *Staphylococcus aureus* (MRSA 272123) and sensitive *Staphylococcus aureus* (ATCC 25928) strains were used as Gram-positive strains. MIC values of compounds were determined in 96-well plates based on the Clinical and Laboratory Standard Institute guidelines (CLSI guidelines).[59] The stock solutions of the compounds (ligands or *in situ* prepared complexes, dissolved in a 90% (v/v) DMSO/H_2O solvent mixture using 10 mM concentration) were diluted in 100 μL of Mueller Hinton Broth, and then two-fold serial dilutions were performed. The starting concentration of the compounds was 100 μM. Then 10^{-4} dilution of an overnight bacterial culture in 100 μL of medium was added to each well, with the exception of the medium control wells. The plates were further incubated at 37 °C for 18 h; at the end of the incubation period, the MIC values of tested compounds were determined by visual inspection.

Conflicts of interest

There are no conflicts to declare.

Data availability

The data supporting this article have been included as part of the supplementary information (SI). Supplementary information: additional ^1H and ^{13}C NMR, ESI-MS, EPR spectra and crystallographic data for characterization and investigation of solution chemical processes. See DOI: https://doi.org/10.1039/d5dt02939b.

CCDC 2512498–2512505 for compounds imidazole-TSC·H_2O, imidazole-Me-TSC, imidazole-Me_2-TSC, imidazole-Me_2-TF·Cl, [Cu(imidazole-TSCH$_{-1}$)Cl]·NaCl·H_2O, [Cu(imidazole-Me-TSC)Cl_2]·0.5H_2O, [Cu(imidazole-Me_2-TSCH$_{-1}$)Cl]·1.5H_2O, [Fe(imidazole-Me_2-TSCH$_{-1}$)$_2$]·Cl·MeOH contain the supplementary crystallographic data for this paper.[60a–h]

Acknowledgements

This work was supported by the National Research Development and Innovation Office (Hungary) through the Slovakian-Hungarian Scientific & Technological Cooperation 2024-1.2.5-TÉT-2024-00056 project, the Slovak Research and Development Agency under contract nos CK49 SK-HU-24-0003 and APVV-23-0195, and COST Action NECTAR (CA18202) supported by COST (European Cooperation in Science and Technology). University of Szeged Open Access Fund (grant number: 8491) is also acknowledged (to É.A.E.).

References

1 D. S. Kalinowski, P. Quach and D. R. Richardson, *Future Med. Chem.*, 2009, **1**, 1143–1151.
2 S. More, P. G. Joshi, Y. K. Mishra and P. K. Khanna, *Mater. Today Chem.*, 2019, **14**, 100195.
3 P. Heffeter, V. F. S. Pape, É.A Enyedy, B. K. Keppler, G. Szakacs and C. R. Kowol, *Antioxid. Redox Signal.*, 2019, **30**, 1062–1082.
4 H. Beraldo and D. Gambino, *Mini-Rev. Med. Chem.*, 2004, **4**, 31–39.
5 A. Miah, K. Harrington and C. Nutting, *Eur. J. Clin. Med. Oncol.*, 2010, **2**, 1.
6 https://www.clinicaltrials.gov (accessed on 07.12.2025).
7 Z. L. Guo, D. R. Richardson, D. S. Kalinowski, Z. Kovacevic, K. C. Tan-Un and G. C. Chan, *J. Hematol. Oncol.*, 2016, **9**, 98.
8 N. A. Seebacher, D. R. Richardson and P. J. Jansson, *Cell Death Dis.*, 2016, **7**, e2510.
9 W. R. Schelman, S. Morgan-Meadows, R. Marnocha, F. Lee, J. Eickhoff, W. Huang, M. Pomplun, Z. Jiang, D. Alberti, J. M. Kolesar, P. Ivy, G. Wilding and A. M. Traynor, *Cancer Chemother. Pharmacol.*, 2009, **63**, 1147–1156.

10 C. Bonaccorso, T. Marzo and D. La Mendola, *Pharmaceuticals*, 2019, **13**, 4.
11 S. Gupta, N. Singh, T. Khan and S. Joshi, *Results Chem.*, 2022, **4**, 100459.
12 F. J. Giles, P. M. Fracasso, H. M. Kantarjian, J. E. Cortes, R. A. Brown, S. Verstovsek, Y. Alvarado, D. A. Thomas, S. Faderl, G. Garcia-Manero, L. P. Wright, T. Samson, A. Cahill, P. Lambert, W. Plunkett, M. Sznol, J. F. DiPersio and V. Gandhi, *Leuk. Res.*, 2003, **27**, 1077.
13 J. Shao, B. Zhou, A. J. Di Bilio, L. Zhu, T. Wang, C. Q. J. Shih and Y. Yen, *Mol. Cancer Ther.*, 2006, **5**, 586.
14 D. B. Lovejoy, P. J. Jansson, U. T. Brunk, J. Wong, P. Ponka and D. R. Richardson, *Cancer Res.*, 2011, **71**, 5871.
15 K. C. Park, L. Fouani, P. J. Jansson, D. Wooi, S. Sahni, D. J. R. Lane, D. Palanimuthu, H. C. Lok, Z. Kovačević, M. L. H. Huang, D. S. Kalinowski and D. R. Richardson, *Metallomics*, 2016, **8**, 874.
16 C. R. Kowol, P. Heffeter, W. Miklos, L. Gille, R. Trondl, L. Cappellacci, W. Berger and B. K. Keppler, *J. Biol. Inorg. Chem.*, 2012, **17**, 409–423.
17 D. X. West and A. E. Liberta, *Coord. Chem. Rev.*, 1993, **123**, 49–71.
18 Z. Zhang, Y. Gou, J. Wang, K. Yang, J. Qi, Z. Zhou, S. Liang, H. Liang and F. Yang, *Eur. J. Med. Chem.*, 2016, **121**, 399–409.
19 M. Belicchi Ferrari, S. Capacchi, G. Pelosi, G. Reffo, P. Tarasconi, R. Albertini, S. Pinelli and P. Lunghi, *Inorg. Chim. Acta*, 1999, **286**, 134–141.
20 S. B. Zahra, A. Khan, N. Ahmed, M. Rafique, L. Fatima, I. Khan, J. Hussain, S. Khalid, H. A. Ogaly, M. M. Ahmed, A. Al-Harrasi and Z. Shafiq, *J. Mol. Struct.*, 2025, **1322**, 140511.
21 V. Singh, V. N. V. Palakkeezhillam, V. Manakkadan, P. Rasin, A. K. Valsan, V. S. Kumar and A. Sreekanth, *Polyhedron*, 2023, **245**, 116658.
22 R. Javahershenas, J. Han, M. Kazemi and P. J. Jervis, *ChemistrySelect*, 2024, **9**, e202401496.
23 Y. Zheng, H. An, J. Qi and J. Li, *Front. Chem.*, 2024, **12**, 1424022.
24 E. Veg, K. Hashmi, M. I. Ahmad, S. Joshi, A. R. Khan and T. Khan, *Nat. Sci.*, 2025, **5**, e70005.
25 O. Palamarciuc, M. N. M. Milunovic, A. Sîrbu, E. Stratulat, A. Pui, N. Gligorijevic, S. Radulovic, J. Kožíšek, D. Darvasiová, P. Rapta, E. A. Enyedy, G. Novitchi, S. Shova and V. B. Arion, *New J. Chem.*, 2019, **43**, 1340–1357.
26 C. R. Kowol, W. Miklos, S. Pfaff, S. Hager, S. Kallus, K. Pelivan, M. Kubanik, É.A Enyedy, W. Berger, P. Heffeter and B. K. Keppler, *J. Med. Chem.*, 2016, **59**, 6739–6752.
27 X. Wang, Y.-F. Chen, W. Yan, L.-L. Cao and Y.-H. Ye, *Molecules*, 2016, **21**, 1574.
28 S. Wang, L. Guan, J. Zang, K. Xing, J. Zhang, D. Liu and L. Zhao, *Molecules*, 2019, **24**, 1198.
29 K. Z. Łączkowski, K. Jachowicz, K. Misiura, A. Biernasiuk and A. Malm, *Heterocycl. Commun.*, 2015, **21**, 109–114.
30 D. Reis, A. Despaigne, J. Silva, N. Silva, C. Vilela, I. Mendes, J. A. Takahashi and H. Beraldo, *Molecules*, 2013, **18**, 12645–12662.
31 É. Frank, Z. Mucsi, I. Zupkó, B. Réthy, G. Falkay, G. Schneider and J. Wölfling, *J. Am. Chem. Soc.*, 2009, **131**, 3894–3904.
32 H. R. Wilson, G. R. Revankar and R. L. Tolman, *J. Med. Chem.*, 1974, **17**, 760–761.
33 V. Pósa, B. Hajdu, G. Tóth, O. Dömötör, C. R. Kowol, B. K. Keppler, G. Spengler, B. Gyurcsik and É. A. Enyedy, *J. Inorg. Biochem.*, 2022, **231**, 111786.
34 O. Dömötör, N. V. May, K. Pelivan, T. Kiss, B. K. Keppler, C. R. Kowol and É.A Enyedy, *Inorg. Chim. Acta*, 2018, **472**, 264–275.
35 S. Hager, V. F. S. Pape, V. Pósa, B. Montsch, L. Uhlik, G. Szakács, S. Tóth, N. Jabronka, B. K. Keppler, C. R. Kowol, É.A Enyedy and P. Heffeter, *Antioxid. Redox Signal.*, 2020, **33**, 395–414.
36 V. Pósa, A. Stefanelli, J. H. B. Nunes, S. Hager, M. Mathuber, N. V. May, W. Berger, B. K. Keppler, C. R. Kowol, É.A Enyedy and P. Heffeter, *Cancers*, 2022, **14**, 4455.
37 T. V. Petrasheuskaya, D. Wernitznig, M. A. Kiss, N. V. May, D. Wenisch, B. K. Keppler, É. Frank and É. A. Enyedy, *J. Biol. Inorg. Chem.*, 2021, **26**, 775–791.
38 T. Gajda, B. Henry and J.-J. Delpuech, *J. Chem. Soc., Dalton Trans.*, 1993, **8**, 1301–1306.
39 P. G. Daniele, O. Zerbinati, V. Zelano and G. Ostacoli, *J. Chem. Soc., Dalton Trans.*, 1991, **10**, 2711–2715.
40 P. J. Morris and R. B. Martin, *J. Inorg. Nucl. Chem.*, 1971, **33**, 2913–2918.
41 É. A. Enyedy, N. V. Nagy, É. Zsigó, C. R. Kowol, V. B. Arion and B. K. Keppler, *Eur. J. Inorg. Chem.*, 2010, **11**, 1717–1728.
42 É. A. Enyedy, É. Zsigó, N. V. Nagy, C. R. Kowol, A. Roller, B. K. Keppler and T. Kiss, *Eur. J. Inorg. Chem.*, 2012, **25**, 4036–4047.
43 É. A. Enyedy, M. F. Primik, C. R. Kowol, V. B. Arion, T. Kiss and B. K. Keppler, *Dalton Trans.*, 2011, **40**, 5895–5905.
44 B. Houari, S. Louhibi, L. Boukli-Hacene, T. Roisnel and M. Taleb, *Acta Crystallogr., Sect. E:Struct. Rep. Online*, 2013, **69**, o1469.
45 S. Gričar, M. Počkaj, G. Marolt, S.Š Bogojević, M. Novinec and J. Kljun, *ChemistrySelect*, 2025, **10**, e202404001.
46 P. Rapta, J. Kožíšek, M. Breza, M. Gembický and L. J. Dunsch, *Electroanal. Chem.*, 2004, **566**, 123–129.
47 CrystalClear SM 1.4.0 Rigaku/MSC Inc. 2008.
48 O. V. Dolomanov, L. J. Bourhis, R. J. Gildea, J. A. K. Howard and H. Puschmann, *J. Appl. Crystallogr.*, 2009, **42**, 339–341.
49 G. M. Sheldrick, *Acta Crystallogr., Sect. A:Found. Adv.*, 2015, **71**, 3–8.
50 L. J. Bourhis, O. V. Dolomanov, R. J. Gildea, J. A. K. Howard and H. Puschmann, *Acta Crystallogr., Sect. A:Found. Adv.*, 2015, **71**, 59–75.

51 C. F. Macrae, P. R. Edgington, P. McCabe, E. Pidcock, G. P. Shields, R. Taylor, M. Towler and J. van De Streek, *J. Appl. Crystallogr.*, 2006, **39**, 453–457.
52 S. P. Westrip, *J. Appl. Crystallogr.*, 2010, **43**, 920–925.
53 T. V. Petrasheuskaya, M. A. Kiss, O. Dömötör, T. Holczbauer, N. V. May, G. Spengler, A. Kincses, A. Čipak Gašparović, É. Frank and É. A. Enyedy, *New J. Chem.*, 2020, **44**, 12154–12168.
54 H. M. Irving, M. G. Miles and L. D. Pettit, *Anal. Chim. Acta*, 1967, **38**, 475–488.
55 P. Gans, A. Sabatini and A. Vacca, *Talanta*, 1996, **43**(10), 1739–1753.
56 L. Zékány and I. Nagypál, in *Computational Methods for the Determination of Stability Constants*, ed. D. L. Leggett, Plenum Press, New York, 1985, p. 291.
57 A. Rockenbauer and L. Korecz, *Appl. Magn. Reson.*, 1996, **10**, 29–43.
58 GraphPad Prism Version 7.00 for Windows Graph Pad Software 2018 https://www.graphpad.com. (accessed 07.12.2025).
59 *Performance Standards for Antimicrobial Susceptibility Testing*, Clinical and Laboratory Standards Institute, Clinical and Laboratory Standards Institute, Wayne, PA, USA, 2018.
60 (*a*) CCDC 2512498: Experimental Crystal Structure Determination, 2026, DOI: 10.5517/ccdc.csd.cc2qbgbw; (*b*) CCDC 2512499: Experimental Crystal Structure Determination, 2026, DOI: 10.5517/ccdc.csd.cc2qbgcx; (*c*) CCDC 2512500: Experimental Crystal Structure Determination, 2026, DOI: 10.5517/ccdc.csd.cc2qbgdy; (*d*) CCDC 2512501: Experimental Crystal Structure Determination, 2026, DOI: 10.5517/ccdc.csd.cc2qbgfz; (*e*) CCDC 2512502: Experimental Crystal Structure Determination, 2026, DOI: 10.5517/ccdc.csd.cc2qbgg0; (*f*) CCDC 2512503: Experimental Crystal Structure Determination, 2026, DOI: 10.5517/ccdc.csd.cc2qbgh1; (*g*) CCDC 2512504: Experimental Crystal Structure Determination, 2026, DOI: 10.5517/ccdc.csd.cc2qbgj2; (*h*) CCDC 2512505: Experimental Crystal Structure Determination, 2026, DOI: 10.5517/ccdc.csd.cc2qbgk3.